Joule

CellPress

Article

Countdown to perovskite space launch: Guidelines to performing relevant radiation-hardness experiments

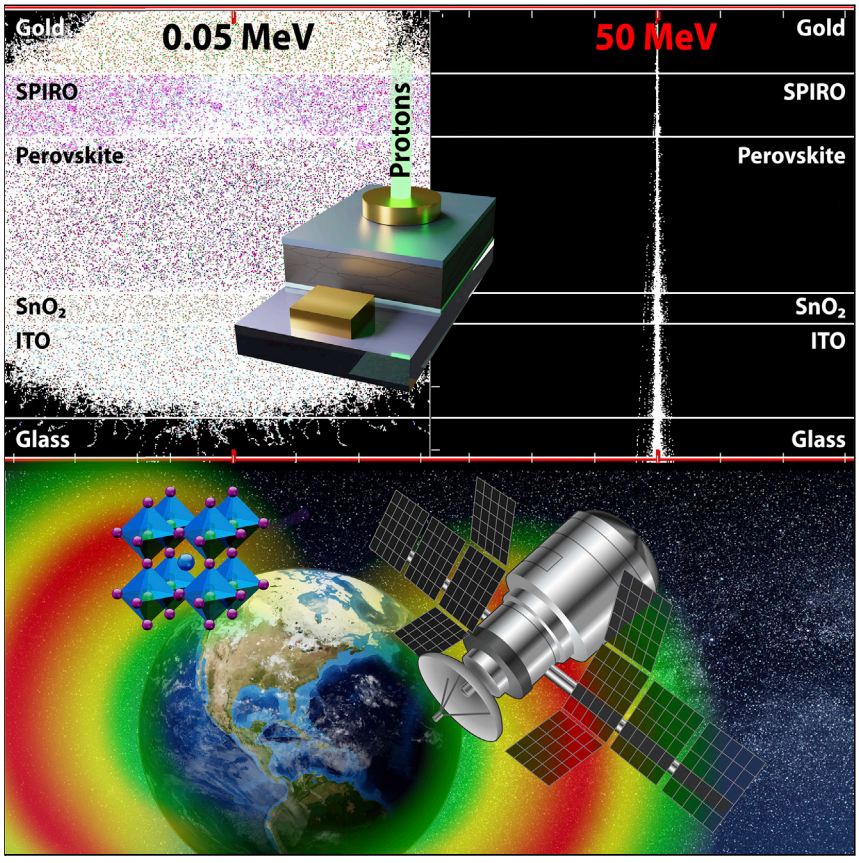

Guidelines for understanding radiation tolerance of perovskite photovoltaics are presented. Based on simulated radiation-matter interactions, low-energy protons (0.05–0.15 MeV) are found to be an optimum radiation source for creating atomic vacancies and therefore probing radiation effects in perovskites. Higher energy protons and electrons create localized heating and can heal defects, making the tests less reliable. These testing protocols are specific to the thicknesses and structure of perovskites and are starkly different from those used for established space photovoltaics.

Ahmad R. Kirmani, Brandon K. Durant, Jonathan Grandidier, ..., David M. Wilt, Kaitlyn T. VanSant, Joseph M. Luther

ahmad.kirmani@nrel.gov (A.R.K.)
joey.luther@nrel.gov (J.M.L.)

Highlights

Radiation-testing protocols are developed and outlined specifically for perovskite PVs

Low-energy protons are critical for understanding perovskite radiation tolerance

High-energy particles can induce lattice healing and add further complexity

Kirmani et al., Joule 6, 1–17
May 18, 2022
https://doi.org/10.1016/j.joule.2022.03.004

Please cite this article in press as: Kirmani et al., Countdown to perovskite space launch: Guidelines to performing relevant radiation-hardness experiments, Joule (2022), https://doi.org/10.1016/j.joule.2022.03.004

Joule

CellPress

Article

Countdown to perovskite space launch: Guidelines to performing relevant radiation-hardness experiments

Ahmad R. Kirmani,[1,*] Brandon K. Durant,[2] Jonathan Grandidier,[3,4] Nancy M. Haegel,[1] Michael D. Kelzenberg,[4] Yao M. Lao,[5] Michael D. McGehee,[6] Lyndsey McMillon-Brown,[7] David P. Ostrowski,[1] Timothy J. Peshek,[7] Bibhudutta Rout,[8] Ian R. Sellers,[2] Mark Steger,[1] Don Walker,[5] David M. Wilt,[9] Kaitlyn T. VanSant,[1,7] and Joseph M. Luther[1,10,*]

SUMMARY

Perovskite photovoltaics (PVs) are under intensive development for promise in terrestrial energy production. Soon, the community will find out how much of that promise may become reality. Perovskites also open new opportunities for lower cost space power. However, radiation tolerance of space environments requires appropriate analysis of relevant devices irradiated under representative radiation conditions. We present guidelines designed to rigorously test the radiation tolerance of perovskite PVs. We review radiation conditions in common orbits, calculate nonionizing and ionizing energy losses (NIEL and IEL) for perovskites, and prioritize proton radiation for effective nuclear interactions. Low-energy protons (0.05–0.15 MeV) create a representative uniform damage profile, whereas higher energy protons (commonly used in ground-based evaluation) require significantly higher fluence to accumulate the equivalent displacement damage dose due to lower scattering probability. Furthermore, high-energy protons may "heal" devices through increased electronic ionization. These procedural guidelines differ from those used to test conventional semiconductors.

INTRODUCTION

As continuing progress pushes metal halide perovskite photovoltaics (PV) toward commercialization for terrestrial solar-to-electricity generation,[1] interest is also rising for beyond-Earth applications.[2] Given their low-cost nature and packaging-enabled high-specific power,[3] lead halide perovskite (of the ABX_3 formula) solar cells can potentially augment the conventional III–V and Si solar panels powering the current generation of satellites. The burgeoning internet of space (IoS) and the expected increase in space PV installation in the low-Earth orbit (LEO) from a current installation of a few MW to ~1 GW over the next decade necessitates a low-cost solar power technology beyond the status quo.[4,5] In fact, a recent comprehensive analysis points toward massive cost reductions of $10–$20 billion USD if perovskite PV is used in the expansion of LEO market instead of the conventional III–V PV.[5] More importantly, although incumbent PV technologies degrade under the severe radiation environment found in space,[6–14] perovskite PV could help herald a new era of space exploration by powering vehicles for long-duration interplanetary missions through extreme radiation environments if perovskite radiation tolerance can meet required demands.[15–18] Future research should focus on demonstrating the

Context & scale

Perovskite solar cells are being actively explored as the next-generation light-weight space photovoltaic technology. Harsh space radiation environment presents a major threat to any in-orbit electronics, necessitating reliable Earth-based space-compatibility testing. We present guidelines that can allow reliable and quick radiation testing of perovskite solar cells using ground-based radiation sources. This consensus article finds that testing protocols established for conventional space photovoltaic technologies based on Si and III–V semiconductors are not applicable for perovskite semiconductors, owing to the latter's soft lattices and markedly different device architectures.

Low-energy protons in the range of 50–150 keV are suggested as the most appropriate radiation to screen perovskite compositions and device architectures for radiation tolerance.

Please cite this article in press as: Kirmani et al., Countdown to perovskite space launch: Guidelines to performing relevant radiation-hardness experiments, Joule (2022), https://doi.org/10.1016/j.joule.2022.03.004

stability of perovskite solar cells under thermal cycling and ultrahigh vacuum conditions,[2] two major challenges that space environments present in addition to harsh radiation.

Perovskite solar cells have recently been launched into the near-Earth space to test compatibility, and the results of these initial experiments are promising.[19–21] To mimic the space radiation environment and explore radiation tolerance of perovskite PV using ground-based testing, multiple research groups have irradiated perovskite solar cells with electrons, protons, gamma radiation, and neutrons.[22–30] These experiments suggest surprisingly high radiation tolerance of perovskites. Huang et al. irradiated formamidinium lead triiodide (FAPI)-based devices with 0.05 MeV (50 keV) protons and found that initial power-conversion efficiencies (PCEs) of 12.3% largely remained unchanged.[22] Sister devices were separately irradiated with 1 MeV electrons and exhibited similar tolerance.[22] Solar cells based on triple-cation perovskite absorbers ($Cs_{0.05}(MA_{0.17}FA_{0.83})_{0.95}Pb(I_{0.83}Br_{0.17})_3$) are currently one of the most stable perovskite compositions with respect to PCEs.[31–33] One of the first attempts at exploring radiation tolerance of these solar cells was performed by Miyazawa et al. using 0.05 MeV protons.[23] Initial PCEs of ~4% remained unchanged even at remarkably high proton fluences of 10^{14} cm^{-2}. These and other reports are summarized in Table 1 and discussed further later.

Although early demonstrations have been used to promote the radiation-tolerance aspect of perovskite PV, the relatively low PCEs of solar cells employed may undermine this claim. This is because low-PCE solar cells likely already have a significant concentration of defect states, and interaction of charged particles with defect-ridden perovskites can result in defect healing, masking the true effect of radiation damage and dosage on the materials and device parameters. Ideally, stable, high-PCE devices should be used for understanding radiation hardness of perovskite PV. Recently, single- and multi-junction solar cells involving perovskites and PCEs >15% have been utilized for some studies; however, as we highlight here, the proton energy ranges used are not representative of the full space environment.[24,25]

When using particle accelerators to perform tests to predict the stability of solar cells in space, it is crucially important to select the right particle energy. Particles that do not have enough energy do not penetrate the cover glass and electrode. However, particles with too much energy transmit through the entire solar cell, causing minimal displacement damage and thus requiring commensurately higher fluences. We show that solar cells made with a ~500-nm-thick metal halide perovskite layer are most effectively tested with protons that have an energy of 0.05–0.15 MeV. These protons create a space-representative uniform damage profile in the cells, although being ~1,000× more damaging than >10 MeV protons. If a cover glass is used, the energy should be increased so that the protons will still maximize damage even after passing through the glass.

Space radiation creates a uniform damage profile in the active regions of III–V solar cells that can be best mimicked in ground-based testing by irradiation with high-energy, fully penetrating protons and using an appropriate fluence to achieve appropriate displacement damage dose (DDD).[36–38] Although radiation-testing protocols and DDD calibrations are well established for conventional space PV technologies, two major characteristics set perovskites apart: thin device stacks (~0.5 μm) and unverified DDD calibrations. Although III–V and Si solar cells require uniform penetration of high-energy protons throughout the device to mimic space radiation

[1]National Renewable Energy Laboratory (NREL), Golden, CO 80215, USA

[2]Homer L. Dodge Department of Physics and Astronomy, University of Oklahoma, 440 W. Brooks St., Norman, OK 73019, USA

[3]Jet Propulsion Laboratory, California Institute of Technology, Pasadena, CA 91109, USA

[4]Department of Applied Physics, California Institute of Technology, Pasadena, CA 91125, USA

[5]Electronic and Photonics Laboratory, The Aerospace Corporation, El Segundo, CA 90245, USA

[6]Materials Science and Engineering, University of Colorado, Boulder, CO 80309, USA

[7]Photovoltaic and Electrochemical Systems Branch, NASA Glenn Research Center, Cleveland, OH 44135, USA

[8]Department of Physics, University of North Texas, Denton, TX 76203, USA

[9]Spacecraft Components Technology Branch (RVSV) US Air Force Research Laboratory, KAFB, Albuquerque, NM, USA

[10]Lead contact

*Correspondence: ahmad.kirmani@nrel.gov (A.R.K.), joey.luther@nrel.gov (J.M.L.)

https://doi.org/10.1016/j.joule.2022.03.004

Please cite this article in press as: Kirmani et al., Countdown to perovskite space launch: Guidelines to performing relevant radiation-hardness experiments, Joule (2022), https://doi.org/10.1016/j.joule.2022.03.004

Table 1. Summary of literature reports on proton irradiation of perovskite solar cells.

Absorber & substrate	Facility & flux (cm^{-2} s^{-1})	Irrad. direction	Perovskite bandgap (eV)	Proton energy (MeV)	Fluence (cm^{-2})	PCE_0/PCE_{irrad}	Year	Ref.
FAPI (*p-i-n*) quartz	Aerospace Corporation, US	top metal	1.47	0.050[a]	1E12	12.3/12.5	2017	22
Triple-cation (*n-i-p*) quartz	Wakasa Wan Energy Research Center, Japan; 3E11	top metal	1.62	0.050[a]	1E12 1E13 1E14 1E15	4.4/4.4 4.4/4.4 4.4/3.3 4.4/2.4	2018	23
MAPI (*p-i-n*) PET	National Institute for Quantum and Radiological Science and Technology (QST), Japan; 3.5E9	top metal	1.54	0.100[a]	3E10 3E12	11/11 11/8.8	2020	34
Triple-cation (*n-i-p*) quartz	Surrey Ion Beam Centre, UK; 3E11	top metal	1.62	0.150[a]	1E13 1E14 1E15	15/12 15/3 15/0.0	2019	35
Triple-cation (*p-i-n*) quartz	Helmholtz-Zentrum Berlin; 9E8	Substrate	1.62	20[b] 68[b]	1E12 1E12	17.0/17.0 18.8/17.9	2019	24
Triple-cation/ CIGS (*Tandem*)	Helmholtz-Zentrum Berlin; 7E8	top IZO	1.62	68[b]	2E12	18/14.9	2020	25
Triple-cation/ Si (*Tandem*)					2E12	21.1/0.18		
Triple-halide (*p-i-n*) quartz	University of North Texas; 1E9–7E10	top ITO	1.70	0.050[a] 0.085[a] 0.300[b] 0.650[b] 1.500[b] 2.500[b]	1E12 1E12 1E12 1E12 1E12 1E12	8.5/6.3 8.4/8.5 9.1/10.1 8.7/9.4 7.9/8.5 8.3/8.4	2021	27

Proton energies marked with the symbol footnote "[a]" are preferred for assessing radiation hardness (as discussed in the text below). Perovskite absorbers are ~500 nm thick. Irradiations is considered in a vacuum of ~1E-5–1E-6 mbar, and the cells have been irradiated for ~1–100 seconds depending on the target proton fluence.

[a]Recommended.

[b]Not recommended.

as highlighted under the Naval Research Laboratory (NRL) radiation-testing protocol,[36,39] we show that such protons are not well suited to testing perovskite cells. Recent studies indicate that the dominant ionizing processes from these protons may lead to healing effects in perovskites that counter the detrimental defects.[27,40] For these reasons, perovskites require a fresh set of radiation-testing conventions. In this paper, we highlight these issues and present a protocol for appropriately evaluating the radiation hardness of perovskites. Perovskites as a space PV technology offers the potential for high-efficiency, low-cost, low-mass, and radiation tolerance. Delivering on that promise will require overcoming all the environmental challenges associated with space operation: thermal cycling, stability under ultraviolet radiation and atomic oxygen, radiation tolerance, and micrometeoroids, etc. This paper focuses on the radiation tolerance challenge and addresses the need to further evaluate radiation-perovskite interactions with rigorous and agreed-upon protocols.

RESULTS AND DISCUSSION

Satellites in space are bombarded with omnidirectional radiation including protons, electrons, neutrons, alpha particles, and gamma rays (Figure 1A). For the near-Earth space, this radiation field is constituted mainly of charged particles from the Sun traveling toward the Earth and trapped by the magnetosphere.[41] For deep space,

Please cite this article in press as: Kirmani et al., Countdown to perovskite space launch: Guidelines to performing relevant radiation-hardness experiments, Joule (2022), https://doi.org/10.1016/j.joule.2022.03.004

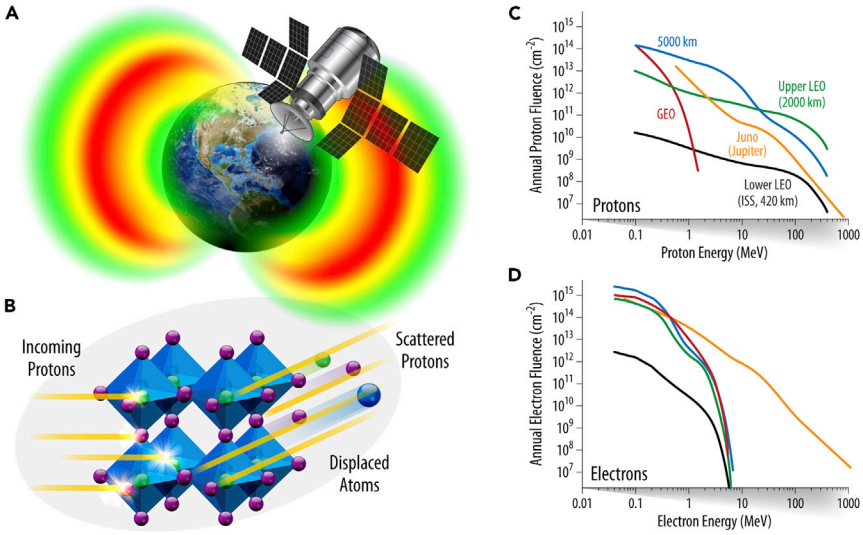

Figure 1. Radiation effects in space orbits

(A) Schematic showing a satellite powered by perovskite solar panels in an Earth orbit and the surrounding radiation field.

(B) Nuclear displacements caused by protons resulting in atomic vacancies.

(C) Simulated annual fluences from the Space Environment Information System (SPENVIS) as a function of proton.

(D) Electron energies for ISS (black), upper-LEO (green), GEO (red), 5,000 km (blue), and Juno (yellow) orbits.

Note: (C) and (D) show integral fluences; visit https://www.spenvis.oma.be/ for differential spectra.

highly energetic galactic cosmic rays form a major component of the radiation field, making interplanetary missions particularly hazardous to on-satellite electronics.

Electrons, protons, and alpha particles are the most prominent sources of radiation in the near-Earth space, and understanding their interactions with a space PV technology is crucial. Although alpha particles cause the most displacement damage due to their high mass (~8,000× electron rest mass), they have the lowest fluence relative to protons and electrons. Protons and electrons, on the other hand, have similar fluences for the near-Earth space orbits, suggesting that both have a similar probability of interacting with a space solar panel. Although there is a 100–1,000× higher electron fluence, protons, given their ~2,000× higher rest mass compared with electrons, inflict significantly more damage.

Interactions of protons and other charged particles with III−V and Si solar cells have been extensively studied in the past. Seminal work by Messenger et al. established protocols for ground-based testing of these cells.[7,8,36,39,42] It was found that an omnidirectional polyenergetic proton flux creates a uniform damage profile inside these devices that can be mimicked by high-energy monoenergetic (1–10 MeV) protons incident normally during ground-based testing.[36] These tests are usually performed by irradiating the III–V and Si solar cells with an equivalent 1 MeV electron fluence, since electron sources are more common than proton sources.[9,11,39,43] This is justified for the case of III–V and Si PV technologies since empirical device performance data show a direct comparison between proton and electron irradiation.[39] Since electrons are not as damaging as protons, as described later, the equivalent 1 MeV electron fluence is usually several orders of magnitude higher than protons to achieve the same level of nuclear displacements. However, such data are not available for perovskites, and the equivalence relations need to be established before

Please cite this article in press as: Kirmani et al., Countdown to perovskite space launch: Guidelines to performing relevant radiation-hardness experiments, Joule (2022), https://doi.org/10.1016/j.joule.2022.03.004

conclusions can be made about using 1 MeV electrons for understanding perovskite PV radiation hardness. Understanding electron-perovskite interactions is important for space orbits dominated by electron fluences such as the geostationary orbit (GEO) and medium-Earth orbit (MEO) as Figure S1 highlights.

Focus on protons

Upon irradiation, protons interact with perovskite films via collisions with atomic nuclei creating vacancies and interstitials (Figure 1B), as has been demonstrated.[27] Depending on their initial energy (E) and direction, protons interact with atoms and lose energy while traveling within the device. Protons losing all energy and stopping within the dimensions of the device (r) cause much more damage since energy loss (dE/dr) is greater at the end of the path. There is a lack of consensus regarding selecting the appropriate proton energy ranges and fluences.[22–25] In Figures 1C and 1D, we present the accumulated annual omnidirectional fluences of particle energies in common space orbits. These include the LEO of International Space Station (ISS), an orbit at the upper limits of LEO at an altitude of 2,000 km (51° inclination), a circular orbit at 5,000 km altitude (60° inclination), GEO, and an extraterrestrial orbit (Juno mission, Jupiter). These data were modeled using SPENVIS,[44] a software developed by the European Space Agency, using the standard AP-8 and AE-8 NASA models for predicting trapped proton and electron environments for Earth orbits, and D&G83 models for the Juno orbit. These calculations do not consider solar proton events that are high fluence ejections of energetic protons into the interplanetary space. Although these solar protons cannot penetrate the magnetospheres, they are expected to heavily impact solar panels during interplanetary missions.

The proton fluence trends highlight that low-energy protons (~0.05 MeV) have a ~10× higher fluence than high-energy protons (>50 MeV) for most of the Earth orbits. From Figure 1D, electrons have a relatively lower energy upper limit (<10 MeV) for Earth orbits, and the electron fluence falls steeply for energies >1 MeV. The ISS orbit is relatively benign and has minimal radiation threat, given its proximity to Earth (~420 km altitude). The orbit of the extraterrestrial Juno mission is of particular interest for radiation-tolerant materials, as extremely energetic electrons and protons (~1 GeV) are present, albeit at very low fluences. Missions to the outer planets may also include a Venus flyby; thus, the cells would need to survive high temperatures. However, since interplanetary missions are expected to involve several years of flight and exploration times, these high-energy particles are expected to become important and can pose unique challenges to perovskite solar panels.

It is important to note that the low-energy proton fluences of $\sim 10^{13}$ cm^{-2} expected for deep-space missions can severely degrade silicon (Si), indium-gallium-phosphide (InGaP), and other III–V solar cells, if these panels are not heavily shielded, as has been previously shown.[16,17] Using encapsulation, such as a cover glass, is a way to mitigate these effects but increases solar array weight and reduces specific power of the panels.

Guidelines for experimental design

As charged particles move through the matter, they lose energy through either nonionizing or ionizing energy loss mechanisms (NIEL and IEL).[45] Although NIEL results in nuclear displacements leading to vacancies and interstitials, IEL causes lattice vibrations and phonon-induced local heating. Understanding the amount of NIEL and IEL at different exposures can help predict the damage inflicted on the solar cell. We simulated the NIELs across proton and electron energies ranges when propagating through hybrid perovskites, all-inorganic perovskites, Si, and InGaP.

Please cite this article in press as: Kirmani et al., Countdown to perovskite space launch: Guidelines to performing relevant radiation-hardness experiments, Joule (2022), https://doi.org/10.1016/j.joule.2022.03.004

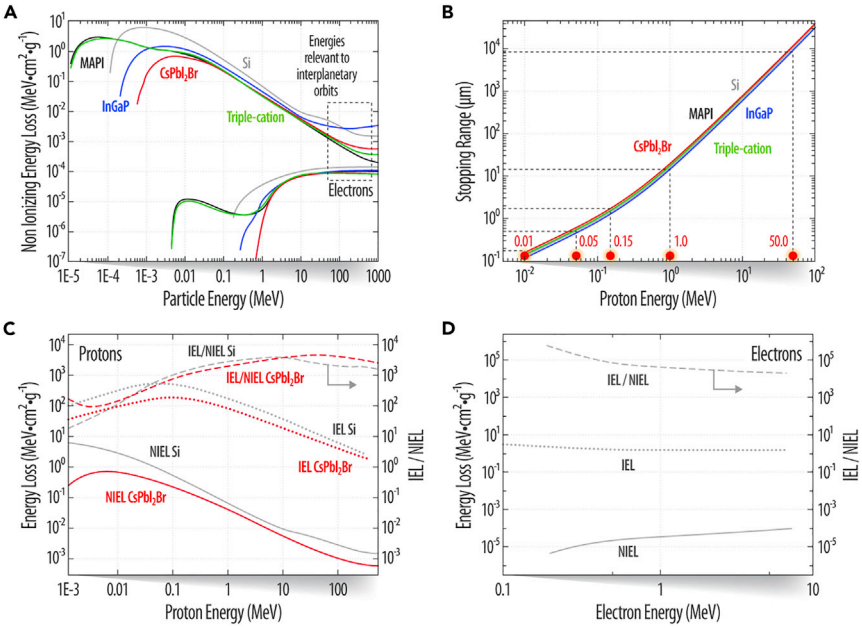

Figure 2. Nonionizing and ionizing energy losses

(A and B) (A) NIELs and (B) stopping ranges of protons for various absorbers. Red circles highlight the proton energies considered for simulating proton-perovskite interactions later.

(C) Proton NIEL, IEL, and the IEL/NIEL ratios for Si (gray) and $CsPbI_2Br$ (red) are shown.

(D) Electron NIEL, IEL, and the IEL/NIEL ratios for Si are shown.

Data shown in (C) and (D) were computed using www.sr-niel.org.

The simulations were done using SPENVIS[44] and verified with an alternate source, SR-NIEL[46] (see Figure S2 for comparison). In general, lower values of NIEL point toward higher radiation resilience. Figure 2A illustrates that protons have NIELs several orders of magnitude higher than electrons for all the materials considered. Low-energy protons (0.05–0.15 MeV) have higher NIEL values compared with high-energy protons (>0.5 MeV). Clearly, protons with energies >10 MeV are ~1,000× less damaging than 0.05–0.15 MeV protons. Electrons have significantly smaller NIEL values. In addition, <1 MeV electrons do not appear to interact with the materials considered here. Electrons penetrate much farther into the device stack yet are far less damaging due to the lower mass of an electron compared with a proton.[22] Importantly, a NIEL peak is observed for electrons with around 0.01 MeV in $Cs_{0.05}(MA_{0.17}FA_{0.83})_{0.95}Pb(I_{0.83}Br_{0.17})_3$ (triple-cation) and $CH_3NH_3PbI_3$ (MAPI) perovskites that is likely due to the presence of the organic A-site. This may explain the sensitivity of hybrid perovskites to SEM and other routine lab experiments that employ such electron energies.

Figure 2A provides a direct comparison of Si and InGaP PV technologies to perovskites. NIEL values of Si are found to be higher than those for perovskite and InGaP due to its lower atomic number than elements in perovskite and InGaP and also because a lower amount of energy is required to displace a Si atom. In contrast, perovskites contain elements with high atomic numbers (Pb and halogens). InGaP is known to possess higher radiation tolerance than Si,[18,47] and can also heal due to photoinjection-enhanced annealing upon illumination.[48–50]

Next, we simulated the stopping ranges of various proton energies in Si, InGaP, and perovskites. The probability of proton scattering increases with the atomic number

Please cite this article in press as: Kirmani et al., Countdown to perovskite space launch: Guidelines to performing relevant radiation-hardness experiments, Joule (2022), https://doi.org/10.1016/j.joule.2022.03.004

(Z) of the target and has an inverse dependence on the proton's velocity. These calculations were done using Stopping and Range of Ions in Matter/Transport of Ions in Matter (SRIM/TRIM).[51] The data are shown in Figure 2B and suggest stopping distances for 0.05 MeV protons are a few hundred nanometers in the perovskites, which is the typical active layer thickness in perovskite solar cells. 0.15 MeV protons will transmit through the perovskite absorbers; however, they can still interact significantly, given that their stopping range is ~1,000 nm. However, >50 MeV protons will require 10 mm of the absorber to completely stop, lose their energy, and result in significant vacancy formation. To achieve appropriate space-relevant defect densities, these protons must be studied at much higher fluence levels than lower energy protons, and in fact, they may locally anneal the perovskite lattice faster than they damage it, as we discuss later.[27,40] These curves also demonstrate that for thicker device stacks such as Si (~100 μm), protons of interest are in the range of 1–10 MeV energies. As such, these curves can be used to tune the incident proton energy depending on the perovskite active layer thickness.

Although work has recently progressed to utilizing high-PCE solar cells for testing radiation tolerance, these reports have exploited >10 MeV protons as a mimic for space radiation (Table 1).[24,25,52] Minimal drop in PCE has then been associated with radiation resilience of perovskites. Although the fluence-energy curves shown in Figure 1C form one piece of evidence suggesting why the choice of such high energies is not ideal, Figures 2A and 2B further amplify this point.

Figure 2C plots the NIEL, IEL, and IEL/NIEL ratio as a function of proton energy for both Si and $CsPbI_2Br$. The ratio becomes significantly higher and plateaus for energies >1 MeV, highlighting that NIEL and IEL scale differently with proton energy. This implies that simply elevating the fluence of high-energy protons to match the NIEL of low-energy protons will not result in equivalent effects considering both nuclear and electronic interactions. Although the two will result in a similar number of vacancies due to nuclear displacements, the former can result in a much greater extent of self-healing due to the increased tendency of electronic ionizations effectively masking the damage due to nonionizing losses.[27,53] Electronic ionization due to high-energy protons has been shown to result in defect passivation in perovskite solar cells likely due to the latter's low defect formation energies, thereby increasing the device performance of the irradiated cells.[27,52] These findings suggest that perovskites are very different in terms of radiation interaction than the conventional technologies.

In fact, the energy loss due to electronic interactions with matter, such as perovskites, is similar to that due to interactions with high-energy protons, resulting in a small number of nuclear displacements.[54] Figure 2D shows NIEL, IEL, and IEL/NIEL for electrons in Si. Since scattering is maximized when masses are matched, electrons have a much higher probability of interaction with electrons in the device stack and lose energy via ionization and subsequent deceleration. The ratio is found to remain constant in the electron energy ranges observed in orbits. A similar healing effect can be expected upon electron irradiation of perovskites, given their soft lattice nature. Therefore, we suggest re-evaluation of electron irradiation of perovskites to understand how meaningful it is for radiation testing of this technology.

Figure S3 shows the DDD values for these PV absorbers. The DDD values are calculated by multiplying the fluences (Figure 1C) and NIELs (Figure 2A). Figure S3B shows these products considering slowed fluences (100-μm-thick cover glass; Figure S1A). As expected, damage caused by the low-energy protons is reduced due to the cover glass. DDD is the energy deposited into 1 g of the material by protons

Please cite this article in press as: Kirmani et al., Countdown to perovskite space launch: Guidelines to performing relevant radiation-hardness experiments, Joule (2022), https://doi.org/10.1016/j.joule.2022.03.004

of a certain incident energy via nonionizing interactions and is a direct representation of the damage caused. Table S1 is a proton look-up table for the ISS orbit. Fluences for 1-, 5-, and 20-year missions are included, along with 1 year DDD for a few PV absorbers of interest. These DDD values enabled us to calculate the 0.1 MeV equivalent annual fluences for the ISS orbit for various PV technologies (Table S2).

Simulating proton-perovskite interactions

Having established the importance of protons as a better probe for testing radiation tolerance of perovskite PV, we proceeded with simulating proton-perovskite interactions. Insights from these simulations, carried out using SRIM/TRIM, are expected to inform experimental design in terms of suitable proton energies to be considered. We considered *n-i-p* solar cells with $Cs_{0.05}(MA_{0.17}FA_{0.83})_{0.95}Pb(I_{0.83}Br_{0.17})_3$ perovskite absorber layers, with the architecture: metal (100 nm)/SPIRO (100 nm)/$Cs_{0.05}(MA_{0.17}FA_{0.83})_{0.95}Pb(I_{0.83}Br_{0.17})_3$ (500 nm)/SnO_2 (50 nm)/ITO (150 nm)/glass (70 nm), based on the thicknesses of various layers in the device stack used commonly in literature and measured using cross-sectional scanning electron microscopy (SEM) (Figure S4) of state-of-the-art cells made in house. A 70-nm-thick glass substrate was assumed to save computational time, since this choice does not impact the simulations as the proton irradiation is done from the metal side. 0.05, 0.15, 1.0, and 50.0 MeV protons were considered.

Figure 3 shows proton-perovskite interactions simulated with SRIM/TRIM. The $Cs_{0.05}(MA_{0.17}FA_{0.83})_{0.95}Pb(I_{0.83}Br_{0.17})_3$ perovskite chemistry results in the state-of-the-art combination of stability, efficiency, and reproducibility in perovskite solar cell research and has been widely studied by the perovskite PV community both for terrestrial applications and radiation tolerance (Table 1). With a bandgap of 1.62 eV, $Cs_{0.05}(MA_{0.17}FA_{0.83})_{0.95}Pb(I_{0.83}Br_{0.17})_3$ is therefore an attractive choice as a single-junction perovskite PV technology for space. Figure 3A shows a device structure and a simulated proton straggling for 0.01 MeV (10 keV) proton radiation. Straggling is defined as the statistical distribution/uncertainity in the projected range of the incident proton beam in both longitudinal and transverse directions as it traverses the device. Protons of energy 0.01 MeV fail to reach the perovskite absorber, even though irradiation was done from the gold electrode side. As shown in Figure S5, the resulting vacancies are limited to the gold electrode.

In Figure 3B, the same simulation is performed with 0.05 MeV protons. As can be seen, these protons are heavily scattered in the perovskite while also fully penetrating the layer, suggesting an ideal condition for radiation testing. As discussed later, protons used for radiation testing should fully penetrate the perovskite layer while creating displacements to mimic the effect of proton radiation found in space. However, even a thin cover glass (1 μm) can effectively block these low-energy protons (Figure 3D). Therefore, if a cover glass is a part of the device stack, energy of the incident protons needs to be accordingly increased, considering the stopping range of protons in the glass. Finally, high-energy protons, such as 1 MeV (Figure 3C), do not significantly interact with the device stack due to low NIELs, and the high IELs can cause joule heating that can result in self-healing by means of thermal annealing. We note that this heating effect is a phenomenon localized in the perovskite lattice due to vibrations caused by interaction of high-energy protons with the electron cloud.[27] This is very different from the heating that is expected for the overall solar panel as the satellite passes the sun and can be managed by using an encapsulant that can block the IR component of sunlight. Additionally, since thermal conductivity of perovskites (0.5 W m^{-1} K^{-1}) is ~100× lower than those of Si (145 W m^{-1} K^{-1}) and

Please cite this article in press as: Kirmani et al., Countdown to perovskite space launch: Guidelines to performing relevant radiation-hardness experiments, Joule (2022), https://doi.org/10.1016/j.joule.2022.03.004

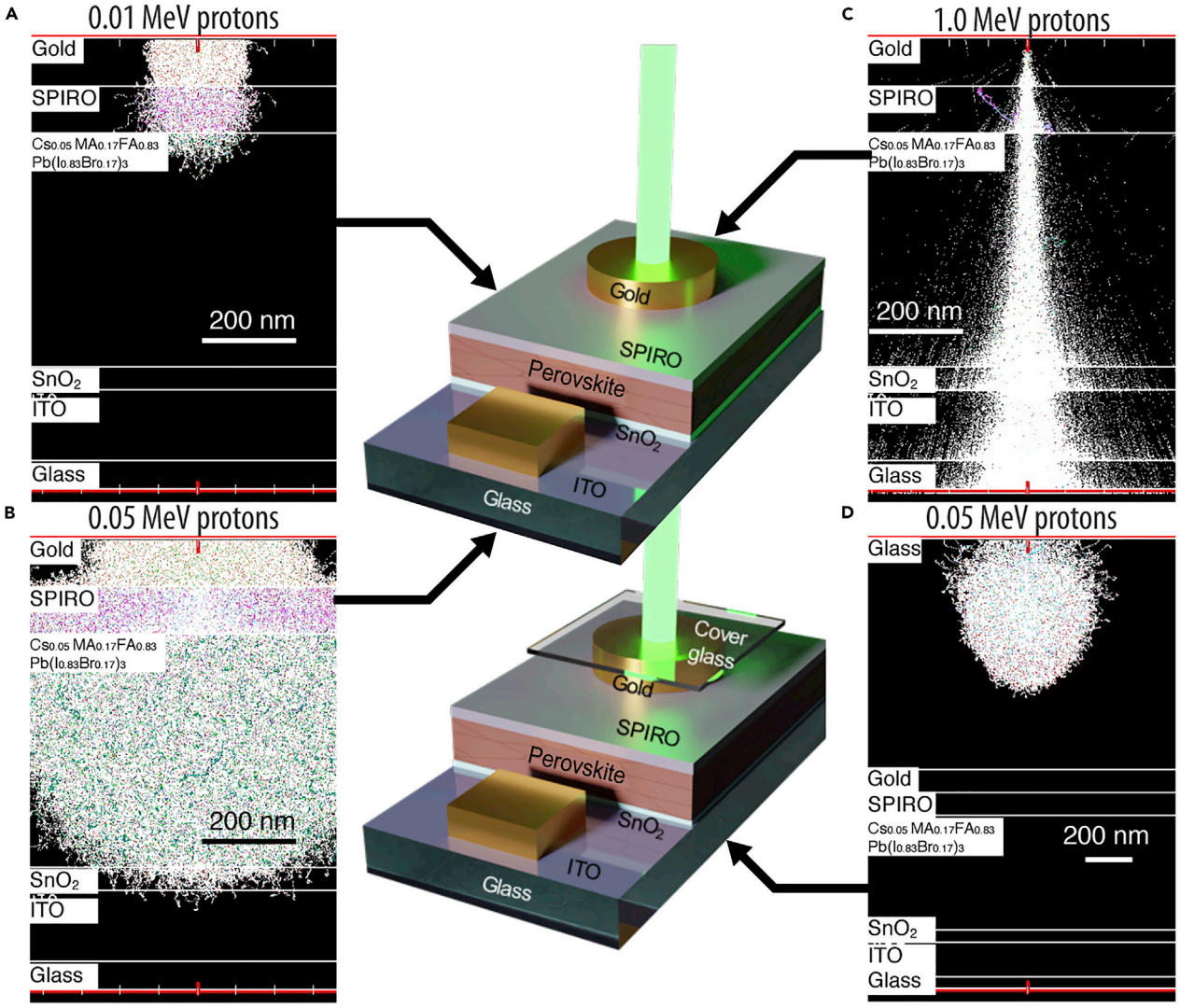

Figure 3. Simulated proton interaction with perovskite devices

(A–D) Various proton-irradiation conditions of the perovskite device stack from the back electrode (Au) side. Normal incidence with (A) 0.01 MeV protons, (B) 0.05 MeV protons, (C) 1.0 MeV protons, and (D) 0.05 MeV protons with a cover glass. Each panel shows a representative device schematic (left) and proton straggling (right). Scale bars, 200 nm. Perovskite absorber layer thickness is 500 nm. A typical cover glass with 100-μm thickness will need ~3.5 MeV proton to pass through the entire depth, with a straggling in the range ~4 μm, making it difficult to study the radiation effects at the perovskite layer alone.

III–V semiconductors (20–80 W m^{-1} K^{-1}),[55,56] these locally produced phonons have a high probability of healing defects before they can be dissipated.

We note that although these harmful low-energy protons can be stopped by a cover glass (Figure 3D), in all cases, higher energy protons get downshifted to the low energies of concern upon passage through the cover glass. Under normal incidence, a ~10-μm-thick cover glass will downshift ~1 MeV protons to energy ranges of 0.05–0.15 MeV by the time they reach the device stack. Although the fluence of 1 MeV protons is lower, upon downshifting to lower energies, they still pose a threat to the device stack due to the higher NIEL values associated with the low energies. In addition, there is a limit to the cover glass thickness as it increases the solar array weight. It is therefore important to understand the interaction of low-energy protons with the device stack since these will

Please cite this article in press as: Kirmani et al., Countdown to perovskite space launch: Guidelines to performing relevant radiation-hardness experiments, Joule (2022), https://doi.org/10.1016/j.joule.2022.03.004

occur even with cover glasses and encapsulants due to energy downshifting. Thus, the most straightforward way to simulate radiation fluences for 10-year missions is proton-irradiation experiments using fluences in the range of 10^{10}–10^{13} cm^{-2}, with proton energies that create a uniform damage profile in the active layer. These experiments should ideally be carried out using proton sources that can produce protons energies in the range of 0.05–0.15 MeV with fluxes of 1E8–1E10 cm^{-2} s^{-1}.

Effects on each atom and uniformity of displacements

Simulated proton straggling for various proton energies and the resulting vacancies due to displacements of C, H, N, Pb, I, Br, and Cs atoms in the perovskite absorber are shown in Figure S6. SRIM/TRIM plots proton tracks as the protons enter and traverse through the device stack, undergoing collisions with each specific atomic nucleus.

We note that for these simulations, protons were normally incident on the device stack to mimic ground-based proton-irradiation conditions. Although space radiation is omnidirectional and the 50 MeV protons are also expected to create more damage in the perovskite stack when incident at grazing incidence angles due to increased path length, such low angles of incidence represent a very small fraction of all the possible incident angles. For example, 50 MeV protons require a path length of 10 mm inside the perovskite device to maximize the defects. This path length will be realized only when these protons are incident at an angle <0.01°. As Figure S7 highlights, >99% of the incident angles are like the normal incidence scenario (angle = 90°) in terms of distance traveled in the device stack, and path lengths start getting longer than the perovskite layer thickness of 500 nm only at very shallow angles.

Figure S8 compares the damage profiles resulting from grazing and normal incidence irradiations of 0.05 and 50 MeV protons on a perovskite solar cell. Although 50 MeV protons interact very weakly with the perovskite at normal incidence, grazing incidence results in ~100× more damage with a uniform profile. As mentioned above, this is due to the increased proton path lengths at low incidence angles. In contrast, grazing incidence of 0.05 MeV protons leads to significantly reduced damage with a nonuniform profile, compared with normal incidence.

Damage profiles for a triple-junction (3J) III–V and a $Cs_{0.05}(MA_{0.17}FA_{0.83})_{0.95}Pb(I_{0.83}Br_{0.17})_3$ perovskite solar cell irradiated with polyenergetic, omnidirectional protons are shown in Figure 4. A slowed proton fluence after passing through a 100-μm-thick cover glass was considered for these simulations. For both cases, a uniform damage profile (black) is observed. Figure 4A shows that the normally incident low-energy protons (0.05 and 0.15 MeV) come to a complete stop within the III–V device stack resulting in a nonuniform damage profile not representative of the space environment, as per the NRL radiation-testing protocol.[36,39] Interestingly, the low-energy protons normally incident on the perovskite solar cell result in a uniform damage profile (Figure 4B). This implies that low-energy protons incident normally from the top metal electrode side of unencapsulated perovskite solar cells can be used to mimic the omnidirectional, polyenergetic space proton radiation in these cells. The reason behind this contrast between perovskites and III–V is the significantly smaller thickness of the perovskite active layers (0.5 μm). Irradiation of a $CsPbI_2Br$ perovskite solar cell with polyenergetic, omnidirectional protons is simulated in Figure S8C with similar conclusions as drawn above for the case of $Cs_{0.05}(MA_{0.17}FA_{0.83})_{0.95}Pb(I_{0.83}Br_{0.17})_3$.

Although higher energy protons also result in uniform damage and are generally preferred for testing conventional PV technologies because of the higher IEL discussed above,[24,27] these should be avoided for the first experiments of determining radiation

Please cite this article in press as: Kirmani et al., Countdown to perovskite space launch: Guidelines to performing relevant radiation-hardness experiments, Joule (2022), https://doi.org/10.1016/j.joule.2022.03.004

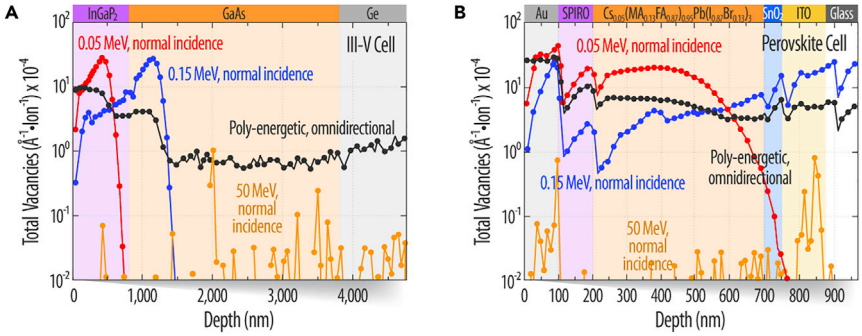

Figure 4. Vacancy creation from proton radiation

(A and B) Damage profiles in (A) triple-junction III–V cell and (B) perovskite cell due to polyenergetic, omnidirectional protons (black), and normally incident low-energy and high-energy protons. Simulations were done using SRIM/TRIM.

tolerance of perovskites.[27,40] The fact that nuclear displacements and electronic ionization scale differently with fluence is further highlighted in Figure S9, where both energy losses are shown for perovskite solar cells for various protons energies. Although a 5,000× higher fluence for 50 MeV protons can equal the nonionizing energy loss via nuclear displacements of that of 0.05 MeV protons, the corresponding loss via electronic ionization is ~100 times higher for these high-energy protons.

We note that conclusions arrived at from these simulations are largely independent of the choice of the perovskite absorber and slight variations in the layer thickness. As an example, we have also simulated proton irradiations of *n-i-p* $CsPbI_2Br$, *n-i-p* $CH_3NH_3PbI_3$, and solar cells with 500-nm-thick perovskite layers. The all-inorganic perovskite chemistry, $CsPbI_2Br$, forms another attractive choice for a space PV absorber, given its wide bandgap of 1.88 eV, high photovoltages (~1.3 V), and the potential for use in multi-junction solar cells.[57–59] $CsPbI_2Br$ can potentially be highly stable at high temperatures and vacuum, has been actively pursued, and high PCEs >17% have been reported.[58,60] Proton straggling and the resulting vacancies for $CsPbI_2Br$ solar cells considering the usually reported 250-nm-thick perovskite absorber layer are shown in Figure S10 with similar conclusions as drawn above for the case of $Cs_{0.05}(MA_{0.17}FA_{0.83})_{0.95}Pb(I_{0.83}Br_{0.17})_3$.

Simulated vacancy profiles for 0.05 MeV proton irradiated *n-i-p* $CH_3NH_3PbI_3$ and *p-i-n* $Cs_{0.05}(MA_{0.17}FA_{0.83})_{0.95}Pb(I_{0.83}Br_{0.17})_3$ cells are shown in Figures S11 and S12 and are nearly identical to the above cases. The reason behind this independence is that a difference of a couple of hundred nanometers in the device thickness and the absorber chemistry does not significantly alter the proton interaction and the choice of the proton energy. We also find that displacemenet of hydrogen (H) is the major contributor to vacancy formation in $Cs_{0.05}(MA_{0.17}FA_{0.83})_{0.95}Pb(I_{0.83}Br_{0.17})_3$ and $CH_3NH_3PbI_3$ due to its prevalence in these lattices, its low displacement energy, and since it has a mass similar to that of a proton (Figures S6 and S11). Interestingly, however, as the proton energy increases (>0.05 MeV), protons start to interact increasingly more with the inorganic framework causing more I vacancies than H, in agreement with previous findings.[24] This is understandable since higher energy protons are much more energetic than H atoms and have a reduced probability of interaction with lower mass atoms. The presence of H in the organic A sites of $CH_3NH_3PbI_3$ and $Cs_{0.05}(MA_{0.17}FA_{0.83})_{0.95}Pb(I_{0.83}Br_{0.17})_3$ absorbers also explain the low-energy NIEL tails observed in Figure 2A for these absorbers. For $CsPbI_2Br$, iodine (I) atomic displacements result in the most vacancies (Figure S10).

Please cite this article in press as: Kirmani et al., Countdown to perovskite space launch: Guidelines to performing relevant radiation-hardness experiments, Joule (2022), https://doi.org/10.1016/j.joule.2022.03.004

Overall, we find differences in vacancy profiles in the device stack by changing the metal electrode and charge transport layers (see Figure S13 and the related discussion). Although it is difficult to draw concrete conclusions, given the low thicknesses of these layers that minimize proton interaction, these results highlight that the choice of the metal electrode and charge extraction layers can also, to some extent, define radiation hardness of the device stack. It should however be noted that defects in charge extraction layers and metal electrode are far less consequential compared with those in the perovskite absorber layer as these layers play little role in the dynamics of the electron-hole pairs photogenerated in the absorber.

Perovskites compared with incumbent technologies

Finally, we sought to compare simulation of the vacancy density of perovskites with incumbent PV technologies, by focusing on proton interactions and looking at vacancy creation. To this end, we considered the following hypothetical device architecture: Au (100 nm)/SPIRO (100 nm)/absorber (250 nm)/SnO_2 (50 nm)/ITO (150 nm)/glass (70 nm). Simulations were carried out for various absorbers of 250 nm thickness: Si, InGaP, $CH_3NH_3PbI_3$, and $Cs_{0.05}(MA_{0.17}FA_{0.83})_{0.95}Pb(I_{0.83}Br_{0.17})_3$ with 0.05 MeV protons. Although Si and InGaP use significantly different device architectures and absorber thicknesses than these assumptions, one can compare them directly using the same thickness and architecture for a materials comparison with perovskites. Results are shown in Figure S14. Si PV undergoes maximum displacements, resulting in the most vacancies, given the low displacement energy of Si and its low atomic number, followed by InGaP. In fact, this trend based on simulations agrees with experimentally observed PCE degradation of irradiated Si and InGaP solar cells. Since active layer thicknesses in conventional solar cells can be several microns with Si PV having ~100-μm-thick absorber, the higher energy proton spectrum gets downshifted to lower energies during passage, further contributing to displacements and device damage. Therefore, higher thicknesses of the conventional PV technologies bring increased radiation damage, besides the extra weight and cost. Further, although cover glasses can stop the low-energy protons, even a 2% offset between the cover glass and Si active area left for the ease of tolerance control during panel assembly resulted in ~15% power loss in Si panels powering previous satellite missions within 77 days of the launch.[11,12] Perovskites, due to the presence of elements with high atomic numbers, such as Pb and halogens, show relatively less vacancy formation, and $CsPbI_2Br$ is found to have the least number of vacancies. The critical link between vacancy formation and radiation hardness depends on the defect tolerance of the material. In general, perovskites are known to perform exceedingly well even with defects due to their remarkable defect tolerance.[61,62] This piece of information points to the need for careful proton-irradiation experiments on various perovskite absorber chemistries and device architectures.

Perovskite PV radiation-testing flowchart

In Figure 5, we summarize the guidelines resulting from the simulations presented in this paper and a review of the literature. Perovskite solar cells chosen for radiation testing should have PCEs approaching or above 20% wherever possible. We prescribe carrying out multiple proton-irradiation tests using a range of low energies (0.05–0.15 MeV) and, appropriate, orbit-relevant fluences. These target the energies of protons when they meet the device stack (top metal electrode), assuming no cover glass is used. If a cover glass is used or the cells are irradiated through the glass that light penetrates during normal operation, energies should be modified accordingly to account for the proton-stopping range in glass. We have provided a look-up table (Table S3) that lists energies that should be used when glass is included. It is also imperative to fabricate perovskite devices on space-relevant substrates for irradiation. For example, soda-lime glass is known to turn brown due to the formation of

Please cite this article in press as: Kirmani et al., Countdown to perovskite space launch: Guidelines to performing relevant radiation-hardness experiments, Joule (2022), https://doi.org/10.1016/j.joule.2022.03.004

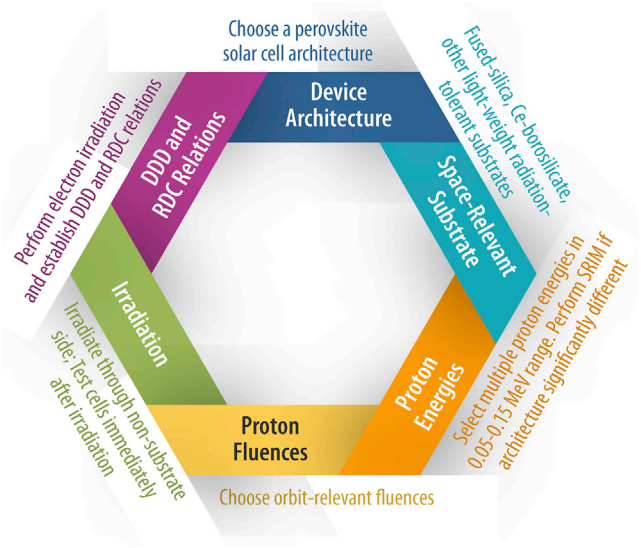

Figure 5. Guidelines flow diagram
Cycle chart summarizing the guidelines to testing radiation hardness of perovskites presented in this paper.

color centers, resulting in the loss of optical transmittance, and it may partially recover transparency over the course of days, confounding PCE quantification.[23,26,63] Devices likely heat up during irradiation, and this effect can either degrade or heal the cell. Device temperature should be monitored during irradiation using a local probe, and temperatures >40°C should be avoided by reducing the particle beam current.

Finally, since the field is still in its infancy, it is not certain that the damage caused in perovskite solar cells due to radiation is entirely due to displacements. To ascertain this, DDD relations and relative damage coefficient (RDC) curves should be established for protons and electrons, as described elaborately for the case of III–V PV.[39] It is important to understand and establish protocols for performance recovery of irradiated perovskite solar cells. For conventional space PV technologies, American Institute of Aeronautics and Astronautics (AIAA) standards include a 60°C anneal and AM0 exposure for performance recovery to replicate recovery typically observed in III–V space PV cells.[64] Attempts at understanding performance recovery in irradiated perovskite solar cells is a welcome step in this direction.[22]

We note that traveler devices should be included as controls for radiation-testing experiments. These devices are not exposed to radiation and serve as controls. However, it is also important to ensure that the devices exhibit long-term shelf-life. This is because it is difficult to factor the travelers' performance degradation into the performance of the irradiated devices. Bathocuproine (BCP) and SPIRO-OMeTAD layers should be avoided wherever possible due to their poor thermal stability and be replaced with more resilient layers. Thermal resilience is a requirement for space-compatible device designs due to thermal cycling in space orbits.

Besides radiation hardness, the other key space challenges that perovskite solar panels will face are thermal cycling, atomic oxygen, ultraviolet photons, vacuum, and micrometeoroids.[2] Future research should also focus on understanding stability of perovskites under these stressors to understand space compatibility.

Please cite this article in press as: Kirmani et al., Countdown to perovskite space launch: Guidelines to performing relevant radiation-hardness experiments, Joule (2022), https://doi.org/10.1016/j.joule.2022.03.004

Conclusions

In summary, we have presented a framework for performing radiation-testing experiments for perovskite PV. Based on particle fluences found in space orbits of interest and NIEL plots, we suggest that protons should be the focus of near-term irradiation experiments. We illustrate that low-energy protons (0.05–0.15 MeV) interact strongly with the perovskite absorbers in typical unencapsulated devices structures, leading to atomic displacements and vacancy formation. Furthermore, the thinness of these devices, their ability to withstand exceptionally high defect densities, and their tendency to self-heal upon irradiation from high-energy particles sets them apart from conventional PV materials that tend to be tested at higher energy or with more the accessible electron sources. We believe that the guidelines presented here will accelerate optimized testing and screening of perovskite PV for radiation tolerance and prepare this exciting technology for liftoff.

EXPERIMENTAL PROCEDURES

Resource availability

Lead contact

Further information and requests for resources and materials should be directed to and will be fulfilled by the lead contact, Joseph Luther (joey.luther@nrel.gov).

Materials availability

This study did not generate new unique materials.

Data and code availability

SPENVIS is available from https://www.spenvis.oma.be/. SRIM/TRIM is available from http://www.srim.org.

SPENVIS calculations

Orbit fluences and NIEL values were simulated using SPENVIS. For Earth orbits, AP-8 and AE-8 models were used, while for the Juno orbit, D&G83 model was used. Parameters for GEO orbit are built into the software; the following parameters were used for the remaining three orbits shown in Figure 1C.

ISS: perigee altitude (km): 417, apogee altitude (km): 422; inclination (deg): 51.64; argument of perigee (deg); 42.17, true anomaly (deg); 130.61

LEO (circular orbit): altitude (km): 2,000; inclination (deg): 51.0

5,000 km (circular orbit): altitude (km): 5,000; inclination (deg): 60.0

Juno: perijove altitude (km): 75,600; apojove altitude (km): 8,100,000; inclination (deg): 90

SRIM/TRIM simulations

SRIM/TRIM simulations were performed considering 100,000 protons for all the cases using the "full damage cascade" calculation mode. *n-i-p* device architectures were considered for irradiation: metal (100 nm)/spiro (100 nm)/absorber (250 nm or 500 nm)/SnO_2 (50 nm)/ITO (150 nm)/glass (70 nm). 250 or 500 nm absorber thickness was used as mentioned in the text. Protons were irradiated from the metal side. A low glass substrate thickness was considered to speed up calculations. Densities used were Au = 19.31 $g.cm^{-3}$, Al = 2.70 $g.cm^{-3}$, Ag = 10.49 $g.cm^{-3}$, SPIRO = 1.40 $g.cm^{-3}$, P3HT = 1.10 $g.cm^{-3}$, $CsPbI_2Br$ = 4.05 $g.cm^{-3}$, $Cs_{0.05}(MA_{0.17}FA_{0.83})_{0.95}Pb(I_{0.83}Br_{0.17})_3$ = 4.30 $g.cm^{-3}$, $CH_3NH_3PbI_3$ = 4.00 $g.cm^{-3}$, SnO_2 = 6.95 $g.cm^{-3}$, TiO_2 = 4.23 $g.cm^{-3}$, ITO = 7.20 $g.cm^{-3}$, glass = 2.53 $g.cm^{-3}$. Displacement energies used were Au = 25 eV,

Al = 25 eV, Ag = 25 eV, C = 28 eV, H = 10 eV, N = 28 eV, O = 28 eV, S = 25 eV, Cs = 25 eV, Pb = 25 eV, I = 25 eV, Br = 25 eV, Si = 15 eV, In = 25 eV, Sn = 25 eV, Ti = 25 eV, Ge = 15 eV, P = 25 eV, As = 25 eV, and Ga = 25 eV. However, since halide ion migration in perovskites is a well-known phenomenon partly responsible for *J-V* hysteresis and phase segregation,[65,66] the values of 25 eV for displacement energies of I and Br are likely an overestimation. The remarkable defect tolerance of perovskites, however, allows the dislocated halide ions to migrate back to their original lattice positions leading to robust optoelectronic properties. Estimation of displacement energies for I and Br in the perovskite lattice is beyond the context of this work.

SRIM simulations for omnidirectional, polyenergetic protons were carried out by changing the incidence angle from 0° (normal) to 89.9° (grazing) in steps of 10°. A total of 100,000 protons were considered and the angle was changed after every 10,000 protons. Within each 10,000-proton bucket, 4 energies were considered: 0.05, 0.15, 1, and 50 MeV. The fluences of these energies were set considering the slowed proton fluence spectrum through a 100-μm cover glass (Figure S1).

SUPPLEMENTAL INFORMATION

Supplemental information can be found online at https://doi.org/10.1016/j.joule.2022.03.004.

ACKNOWLEDGMENTS

This work was authored in part by the National Renewable Energy Laboratory, operated by Alliance for Sustainable Energy, LLC, for the U.S. Department of Energy (DOE) under contract no. DE-AC36-08GO28308. NREL acknowledges support from the Operational Energy Capability Improvement Fund (OECIF) of the U.S. Department of Defense (DOD). Part of this research was carried out at the Jet Propulsion Laboratory, California Institute of Technology, under a contract with the National Aeronautics and Space Administration (80NM0018D0004). B.R. acknowledges partial support from NSF grant number HBCU-EiR-2101181. M.D.K. is supported by the Space Solar Power Project at Caltech. NASA authors acknowledge funding provided by the Early Career Initiative Program within NASA's Space Technology Mission Directorate. The work at the University of Oklahoma is supported by NASA under agreement no. 80NSSC19M0140 issued through NASA Oklahoma EPSCoR. The authors wish to thank R. Darling of the Office of the Undersecretary of Defense for Acquisition and Sustainment, Arlington, VA, USA, for guidance and support. The views expressed in the article do not necessarily represent the views of the DOE or the U.S. Government.

AUTHOR CONTRIBUTIONS

A.R.K. and J.M.L. conceived and supervised this work and wrote the manuscript. A.R.K. carried out all the SRIM/TRIM and NIEL, IEL simulations after in-depth discussions with D.W., B.R., D.M.W., B.K.D, and M.S. All authors contributed to the discussion and editing of the manuscript.

DECLARATION OF INTERESTS

M.D.M. is an advisor to Swift Solar and a member of the *Joule* advisory board.

Received: November 10, 2021
Revised: February 8, 2022
Accepted: March 16, 2022
Published: April 11, 2022

REFERENCES

1. Berry, J.J., van de Lagemaat, J., Al-Jassim, M.M., Kurtz, S., Yan, Y., and Zhu, K. (2017). Perovskite photovoltaics: the path to a printable terawatt-scale technology. ACS Energy Lett. *2*, 2540–2544. https://doi.org/10.1021/acsenergylett.7b00964.

2. Tu, Y., Wu, J., Xu, G., Yang, X., Cai, R., Gong, Q., Zhu, R., and Huang, W. (2021). Perovskite solar cells for space applications: progress and challenges. Adv. Mater. *33*, e2006545. https://doi.org/10.1002/adma.202006545.

3. Kaltenbrunner, M., Adam, G., Głowacki, E.D., Drack, M., Schwödiauer, R., Leonat, L., Apaydin, D.H., Groiss, H., Scharber, M.C., White, M.S., et al. (2015). Flexible high power-per-weight perovskite solar cells with chromium oxide–metal contacts for improved stability in air. Nat. Mater. *14*, 1032–1039. https://doi.org/10.1038/nmat4388.

4. Akyildiz, I.F., and Kak, A. (2019). The Internet of space things/CubeSats. IEEE Network *33*, 212–218. https://doi.org/10.1109/MNET.2019.1800445.

5. Ho-Baillie, A.W.Y., Sullivan, H.G.J., Bannerman, T.A., Talathi, H.P., Bing, J., Tang, S., Xu, A., Bhattacharyya, D., Cairns, I.H., and McKenzie, D.R. (2022). Deployment opportunities for space photovoltaics and the prospects for perovskite solar cells. Adv. Mater. Technol. *7*. https://doi.org/10.1002/admt.202101059.

6. Sharps, P.R., Aiken, D.J., Stan, M.A., Thang, C.H., and Fatemi, N. (2002). Proton and electron radiation data and analysis of $GaInP_2$/GaAs/Ge solar cells. Prog. Photovolt.: Res. Appl. *10*, 383–390. https://doi.org/10.1002/pip.444.

7. Messenger, S.R., Burke, E.A., Morton, T.L., Summers, G.P., Walters, R.J., and Warner, J.H. (2003). Modelling low energy proton radiation effects on solar cells. Proceedings of the 3rd World Conference on Photovoltaic Energy Conversion, *711*, pp. 716–719.

8. Messenger, S.R., Burke, E.A., Lorentzen, J.R., Walters, R.J., Warner, J.H., Summers, G.P., and Taylor, S.J. (2005). Quantifying low energy proton damage in multijunction solar cells. In Proceedings of the 19th Space Photovoltaic Research and Technology Conference, p. 77.

9. Anspaugh, B.E. (1991). Proton and electron damage coefficients for GaAs/Ge solar cells. The Conference Record of the Twenty-Second IEEE Photovoltaic Specialists Conference, *1592*, pp. 1593–1598.

10. Shen, X.B., Aierken, A., Heini, M., Mo, J.H., Lei, Q.Q., Zhao, X.F., Sailai, M., Xu, Y., Tan, M., Wu, Y.Y., et al. (2019). Degradation analysis of 1 MeV electron and 3 MeV proton irradiated InGaAs single junction solar cell. AIP Adv. *9*, 075205. https://doi.org/10.1063/1.5094472.

11. Curtin, D.J., and Statler, R.L. (1975). Review of radiation damage to silicon solar cells. IEEE Trans. Aerosp. Electron. Syst. *AES–11*, 499–513. https://doi.org/10.1109/TAES.1975.308112.

12. Statler, R.L., and Curtin, D.J. (1971). Radiation damage in silicon solar cells from low-energy protons. IEEE Trans. Electron Devices *18*, 412–417. https://doi.org/10.1109/T-ED.1971.17217.

13. Ohshima, T., S.I.S., Nakamura, T., Imaizumi, M., Sugaya, T., Matsubara, K., Niki, S., Takeda, A., and Okano, Y. (2013). Electrical performance degradation of GaAs solar cells with InGaAs quantum dot layers due to proton irradiation. IEEE 39th PVSC. 2779-2783. doi: 10.1109/PVSC.2013.6745049.

14. Burgess, R.M., W.S.C., Devaney, W.E., Doyle, D.H., Kim, N.P., and Stanbery, B.J. (1988). Electron and proton radiation effects on GaAs and CuInSe2 thin film solar cells. 20th IEEE Photovoltaic Specialists Conference. 909-912.

15. Markvart, T. (1990). Radiation damage in solar cells. J. Mater. Sci.: Mater. Electron. *1*, 1–12. https://doi.org/10.1007/BF00716008.

16. Imaizumi, M., Nakamura, T., Takamoto, T., Ohshima, T., and Tajima, M. (2017). Radiation degradation characteristics of component subcells in inverted metamorphic triple-junction solar cells irradiated with electrons and protons. Prog. Photovolt.: Res. Appl. *25*, 161–174. https://doi.org/10.1002/pip.2840.

17. Sumita, T., Imaizumi, M., Matsuda, S., Ohshima, T., Ohi, A., and Itoh, H. (2003). Proton radiation analysis of multi-junction space solar cells. Nucl. Instrum. Methods Phys. Res. B: Beam Interact. Mater. At. *206*, 448–451. https://doi.org/10.1016/S0168-583X(03)00791-2.

18. Gruginskie, N., Cappelluti, F., Bauhuis, G.J., Mulder, P., Haverkamp, E.J., Vlieg, E., and Schermer, J.J. (2020). Electron radiation–induced degradation of GaAs solar cells with different architectures. Prog. Photovolt.: Res. Appl. *28*, 266–278. https://doi.org/10.1002/pip.3224.

19. Cardinaletti, I., Vangerven, T., Nagels, S., Cornelissen, R., Schreurs, D., Hruby, J., Vodnik, J., Devisscher, D., Kesters, J., D'Haen, J., et al. (2018). Organic and perovskite solar cells for space applications. Sol. Energy Mater. Sol. Cells *182*, 121–127. https://doi.org/10.1016/j.solmat.2018.03.024.

20. Tu, Y., Xu, G., Yang, X., Zhang, Y., Li, Z., Su, R., Luo, D., Yang, W., Miao, Y., Cai, R., et al. (2019). Mixed-cation perovskite solar cells in space. Sci. China: Phys., Mech. Astron. *62*, 1–4. https://doi.org/10.1007/s11433-019-9356-1.

21. Reb, L.K., Böhmer, M., Predeschly, B., Grott, S., Weindl, C.L., Ivandekic, G.I., Guo, R., Dreißigacker, C., Gernhäuser, R., Meyer, A., et al. (2020). Perovskite and organic solar cells on a rocket flight. Joule *4*, 1880–1892. https://doi.org/10.1016/j.joule.2020.07.004.

22. Huang, J., Kelzenberg, M.D., Espinet-González, P., Mann, C., Walker, D., Naqavi, A., Vaidya, N., Warmann, E., and Atwater, H.A. (2017). Effects of electron and proton radiation on perovskite solar cells for space solar power application. In Proceedings of the 2017 IEEE 44th Photovoltaic Specialist Conference (PVSC), pp. 1248–1252.

23. Miyazawa, Y., Ikegami, M., Chen, H.W., Ohshima, T., Imaizumi, M., Hirose, K., and Miyasaka, T. (2018). Tolerance of perovskite solar cell to high-energy particle irradiations in space environment. iScience *2*, 148–155. https://doi.org/10.1016/j.isci.2018.03.020.

24. Lang, F., Jošt, M., Bundesmann, J., Denker, A., Albrecht, S., Landi, G., Neitzert, H.-C., Rappich, J., and Nickel, N.H. (2019). Efficient minority carrier detrapping mediating the radiation hardness of triple-cation perovskite solar cells under proton irradiation. Energy Environ. Sci. *12*, 1634–1647. https://doi.org/10.1039/C9EE00077A.

25. Lang, F., Jošt, M., Frohna, K., Köhnen, E., Al-Ashouri, A., Bowman, A.R., Bertram, T., Morales-Vilches, A.B., Koushik, D., Tennyson, E.M., et al. (2020). Proton radiation hardness of perovskite tandem photovoltaics. Joule *4*, 1054–1069. https://doi.org/10.1016/j.joule.2020.03.006.

26. Yang, S., Xu, Z., Xue, S., Kandlakunta, P., Cao, L., and Huang, J. (2019). Organohalide lead perovskites: more stable than glass under gamma-ray radiation. Adv. Mater. *31*, e1805547. https://doi.org/10.1002/adma.201805547.

27. Durant, B.K., Afshari, H., Singh, S., Rout, B., Eperon, G.E., and Sellers, I.R. (2021). Tolerance of perovskite solar cells to targeted proton irradiation and electronic ionization induced healing. ACS Energy Lett. *6*, 2362–2368. https://doi.org/10.1021/acsenergylett.1c00756.

28. Boldyreva, A.G., Akbulatov, A.F., Tsarev, S.A., Luchkin, S.Y., Zhidkov, I.S., Kurmaev, E.Z., Stevenson, K.J., Petrov, V.G., and Troshin, P.A. (2019). γ-ray-induced degradation in the triple-cation perovskite solar cells. J. Phys. Chem. Lett. *10*, 813–818. https://doi.org/10.1021/acs.jpclett.8b03222.

29. Paternò, G.M., Robbiano, V., Santarelli, L., Zampetti, A., Cazzaniga, C., Garcia Sakai, V., and Cacialli, F. (2019). Perovskite solar cell resilience to fast neutrons. Sustainable Energy Fuels *3*, 2561–2566. https://doi.org/10.1039/C9SE00102F.

30. Miyazawa, Y., Ikegami, M., Miyasaka, T., Ohshima, T., Imaizumi, M., and Hirose, K. (2015). Evaluation of radiation tolerance of perovskite solar cell for use in space. In Proceedings of the 2015 IEEE 42nd Photovoltaic Specialist Conference (PVSC), pp. 1–4.

31. Christians, J.A., Schulz, P., Tinkham, J.S., Schloemer, T.H., Harvey, S.P., Tremolet de Villers, B.J., Sellinger, A., Berry, J.J., and Luther, J.M. (2018). Tailored interfaces of unencapsulated perovskite solar cells for >1,000 hour operational stability. Nat. Energy *3*, 68–74. https://doi.org/10.1038/s41560-017-0067-y.

32. Schloemer, T.H., Gehan, T.S., Christians, J.A., Mitchell, D.G., Dixon, A., Li, Z., Zhu, K., Berry, J.J., Luther, J.M., and Sellinger, A. (2019). Thermally stable perovskite solar cells by systematic molecular design of the hole-transport layer. ACS Energy Lett. *4*, 473–482. https://doi.org/10.1021/acsenergylett.8b02431.

33. Saliba, M., Matsui, T., Seo, J.Y., Domanski, K., Correa-Baena, J.P., Nazeeruddin, M.K., Zakeeruddin, S.M., Tress, W., Abate, A.,

Hagfeldt, A., et al. (2016). Cesium-containing triple cation perovskite solar cells: improved stability, reproducibility and high efficiency. Energy Environ. Sci. *9*, 1989–1997. https://doi.org/10.1039/C5EE03874J.

34. Malinkiewicz, O., Imaizumi, M., Sapkota, S.B., Ohshima, T., and Öz, S. (2020). Radiation effects on the performance of flexible perovskite solar cells for space applications. Emerg. Mater. Res. *3*, 9–14. https://doi.org/10.1007/s42247-020-00071-8.

35. Barbé, J., Hughes, D., Wei, Z., Pockett, A., Lee, H.K.H., Heasman, K.C., Carnie, M.J., Watson, T.M., and Tsoi, W.C. (2019). Radiation hardness of perovskite solar cells based on aluminum-doped zinc oxide electrode Under proton irradiation. Sol. RRL *3*, 1900219. https://doi.org/10.1002/solr.201900219.

36. Messenger, S.R., Burke, E.A., Walters, R.J., Warner, J.H., Summers, G.P., and Morton, T.L. (2006). Effect of omnidirectional proton irradiation on shielded solar cells. IEEE Trans. Nucl. Sci. *53*, 3771–3778. https://doi.org/10.1109/TNS.2006.886220.

37. Summers, G.P., Walters, R.J., Xapsos, M.A., Burke, E.A., Messenger, S.R., Shapiro, P., and Statler, R.L. (1994). A New Approach to Damage Prediction for Solar Cells Exposed to Different Radiations. Proceedings of 1994 IEEE 1st World Conference on Photovoltaic Energy Conversion-WCPEC (A Joint Conference of PVSC, PVSEC and PSEC), *2062*, pp. 2068–2075.

38. Summers, G.P., Burke, E.A., and Xapsos, M.A. (1995). Displacement damage analogs to ionizing radiation effects. Radiat. Meas. *24*, 1–8. https://doi.org/10.1016/1350-4487(94)00093-G.

39. Messenger, S.R., Summers, G.P., Burke, E.A., Walters, R.J., and Xapsos, M.A. (2001). Modeling solar cell degradation in space: A comparison of the NRL displacement damage dose and the JPL equivalent fluence approaches. Prog. Photovolt.: Res. Appl. *9*, 103–121. https://doi.org/10.1002/pip.357.

40. Durant, B.K., Afshari, H., Sourabh, S., Yeddu, V., Bamidele, M.T., Singh, S., Rout, B., Eperon, G.E., Kim, D.Y., and Sellers, I.R. (2021). Radiation stability of mixed tin–lead halide perovskites: implications for space applications. Sol. Energy Mater. Sol. Cells *230*, 111232. https://doi.org/10.1016/j.solmat.2021.111232.

41. Gao, X., Y.S., and Feng, Z. (2014). Radiation effects of space solar cells. In High-Efficiency Solar Cells (Springer), pp. 597–622. https://doi.org/10.1007/978-3-319-01988-8_20.

42. Messenger, S.R., Burke, E.A., Summers, G.P., Xapsos, M.A., Walters, R.J., Jackson, E.M., and Weaver, B.D. (1999). Nonionizing energy loss (NIEL) for heavy ions. IEEE Trans. Nucl. Sci. *46*, 1595–1602. https://doi.org/10.1109/23.819126.

43. Kurtz, S., King, R.R., Edmondson, K.M., Friedman, D.J., and Karam, N.H. (2002). 1-MeV-Electron Irradiation of GaInAsN Cells. In Proceedings of the Conference Record of the Twenty-Ninth IEEE Photovoltaic Specialists Conference, pp. 1006–1009.

44. https://www.spenvis.oma.be/.

45. Campesato, R., Baur, C., Casale, M., Gervasi, M., Gombia, E., Greco, E., Kingma, A., Rancoita, P.G., Rozza, D., and Tacconi, M. (2018). NIEL DOSE and DLTS analyses on triple and single junction solar cells irradiated with electrons and protons. In Proceedings of the 2018 IEEE 7th World Conference on Photovoltaic Energy Conversion (WCPEC) (A Joint Conference of 45th IEEE PVSC, 28th PVSEC & 34th EU PVSEC), pp. 3768–3772.

46. http://www.sr-niel.org/.

47. Imaizumi, M., Taylor, S.J., Yamaguchi, M., Ito, T., Hisamatsu, T., and Matsuda, S. (1999). Analysis of structure change of Si solar cells irradiated with high fluence electrons. J. Appl. Phys. *85*, 1916–1920. https://doi.org/10.1063/1.369184.

48. Yamaguchi, M., and Ando, K. (1988). Mechanism for radiation resistance of InP solar cells. J. Appl. Phys. *63*, 5555–5562. https://doi.org/10.1063/1.340332.

49. Yamaguchi, M., Ando, K., Yamamoto, A., and Uemura, C. (1984). Minority-carrier injection annealing of electron irradiation-induced defects in InP solar cells. Appl. Phys. Lett. *44*, 432–434. https://doi.org/10.1063/1.94756.

50. Yamaguchi, M., Okuda, T., and Taylor, S.J. (1997). Minority-carrier injection-enhanced annealing of radiation damage to InGaP solar cells. Appl. Phys. Lett. *70*, 2180–2182. https://doi.org/10.1063/1.119034.

51. Ziegler, J.F., Ziegler, M.D., and Biersack, J.P. (2010). SRIM – the stopping and range of ions in matter. Nucl. Instrum. Methods Phys. Res. B: Beam Interact. Mater. At. *268*, 1818–1823. https://doi.org/10.1016/j.nimb.2010.02.091.

52. Brus, V.V., Lang, F., Bundesmann, J., Seidel, S., Denker, A., Rech, B., Landi, G., Neitzert, H.C., Rappich, J., and Nickel, N.H. (2017). Defect dynamics in proton irradiated CH3NH3PbI3 perovskite solar cells. Adv. Electron. Mater. *3*, 1600438. https://doi.org/10.1002/aelm.201600438.

53. Afshari, H., Durant, B.K., Thrasher, T., Abshire, L., Whiteside, V.R., Chan, S., Kim, D., Hatch, S., Tang, M., McNatt, J.S., et al. (2021). Radiation tolerance of GaAs1-xSbx solar cells. Sol. Energy Mater. Sol. Cells *233*, 111352. https://doi.org/10.1016/j.solmat.2021.111352.

54. Nikjoo, H., Uehara, S., and Emfietzoglou, D. (2016). Interaction of Radiation With Matter (CRC Press).

55. Heiderhoff, R., Haeger, T., Pourdavoud, N., Hu, T., Al-Khafaji, M., Mayer, A., Chen, Y., Scheer, H.-C., and Riedl, T. (2017). Thermal conductivity of methylammonium lead halide perovskite single crystals and thin films: A comparative study. J. Phys. Chem. C *121*, 28306–28311. https://doi.org/10.1021/acs.jpcc.7b11495.

56. Maycock, P.D. (1967). Thermal conductivity of silicon, germanium, III–V compounds and III–V alloys. Sol. State Electron. *10*, 161–168. https://doi.org/10.1016/0038-1101(67)90069-X.

57. Wang, M., Cao, F., Wang, M., Deng, K., and Li, L. (2021). Intermediate-adduct-assisted growth of stable $CsPbI_2Br$ inorganic perovskite films for high-efficiency semitransparent solar cells. Adv. Mater. *33*, e2006745. https://doi.org/10.1002/adma.202006745.

58. He, J., Liu, J., Hou, Y., Wang, Y., Yang, S., and Yang, H.G. (2020). Surface chelation of cesium halide perovskite by dithiocarbamate for efficient and stable solar cells. Nat. Commun. *11*, 4237. https://doi.org/10.1038/s41467-020-18015-5.

59. Beal, R.E., Slotcavage, D.J., Leijtens, T., Bowring, A.R., Belisle, R.A., Nguyen, W.H., Burkhard, G.F., Hoke, E.T., and McGehee, M.D. (2016). Cesium lead halide perovskites with improved stability for tandem solar cells. J. Phys. Chem. Lett. *7*, 746–751. https://doi.org/10.1021/acs.jpclett.6b00002.

60. Luo, Y.-X., Xie, F.-M., Chen, J.-D., Ren, H., Wang, J.-K., Cai, X.-Y., Shen, K.-C., Lu, L.-Y., Li, Y.-Q., Luponosov, Y.N., et al. (2021). Uniform stepped interfacial energy level structure boosts efficiency and stability of $CsPbI_2Br$ solar cells. Adv. Funct. Mater. *31*, 2103316. https://doi.org/10.1002/adfm.202103316.

61. Ball, J.M., and Petrozza, A. (2016). Defects in perovskite-halides and their effects in solar cells. Nat. Energy *1*, 16149. https://doi.org/10.1038/nenergy.2016.149.

62. Brandt, R.E., Poindexter, J.R., Gorai, P., Kurchin, R.C., Hoye, R.L.Z., Nienhaus, L., Wilson, M.W.B., Polizzotti, J.A., Sereika, R., Žaltauskas, R., et al. (2017). Searching for "defect-tolerant" photovoltaic materials: combined theoretical and experimental screening. Chem. Mater. *29*, 4667–4674. https://doi.org/10.1021/acs.chemmater.6b05496.

63. El-Kheshen, A.A. (2012). Glass as Radiation Sensor. In Current Topics in Ionizing Radiation Research (IntechOpen).

64. Plus, P.D. (2019). Qualification and quality requirements for space solar cells—Amendment 1, S-111A–S-2014/A1-2019.

65. Knight, A.J., and Herz, L.M. (2020). Preventing phase segregation in mixed-halide perovskites: a perspective. Energy Environ. Sci. *13*, 2024–2046. https://doi.org/10.1039/D0EE00788A.

66. Elmelund, T., Seger, B., Kuno, M., and Kamat, P.V. (2020). How interplay between photo and thermal activation dictates halide ion segregation in mixed halide perovskites. ACS Energy Lett. *5*, 56–63. https://doi.org/10.1021/acsenergylett.9b02265.

Joule, Volume *6*

Supplemental information

Countdown to perovskite space launch:

Guidelines to performing

relevant radiation-hardness experiments

Ahmad R. Kirmani, Brandon K. Durant, Jonathan Grandidier, Nancy M. Haegel, Michael D. Kelzenberg, Yao M. Lao, Michael D. McGehee, Lyndsey McMillon-Brown, David P. Ostrowski, Timothy J. Peshek, Bibhudutta Rout, Ian R. Sellers, Mark Steger, Don Walker, David M. Wilt, Kaitlyn T. VanSant, and Joseph M. Luther

Supplementary Information
Countdown to perovskite Space launch: *Guidelines to performing relevant radiation-hardness experiments*

Ahmad R. Kirmani[1,], Brandon K. Durant[2], Jonathan Grandidier[3], Nancy Haegel[1], Michael D. Kelzenberg[4], Yao M. Lao[5], Michael D. McGehee[6], Lyndsey McMillon-Brown[7], David P. Ostrowski[1], Timothy J. Peshek[7], Bibhudutta Rout[8], Ian R. Sellers[2], Mark Steger[1], Don Walker[5], David M. Wilt[9], Kaitlyn T. VanSant[1,7], and Joseph M. Luther[1,*]*

[1]National Renewable Energy Laboratory (NREL), CO 80215, USA
[2]Homer L. Dodge Department of Physics and Astronomy, University of Oklahoma, 440 W. Brooks St, Norman, OK, 73019, USA
[3]Jet Propulsion Laboratory, California Institute of Technology, Pasadena, CA 91109, USA
[4]Department of Applied Physics, California Institute of Technology, Pasadena CA, 91125, USA
[5]Electronic and Photonics Laboratory, The Aerospace Corporation, El Segundo, CA 90245, USA
[6]Materials Science and Engineering, University of Colorado, Boulder, CO, 80309, USA
[7]Photovoltaic and Electrochemical Systems Branch, NASA Glenn Research Center, Cleveland, OH 44135, USA
[8]Department of Physics, University of North Texas, Denton, TX 76203, USA
[9]Spacecraft Components Technology Branch (RVSV) US Air Force Research Laboratory, KAFB NM, USA
[*]Corresponding Authors: ahmad.kirmani@nrel.gov, joey.luther@nrel.gov
LEAD CONTACT: Joseph Luther, joey.luther@nrel.gov

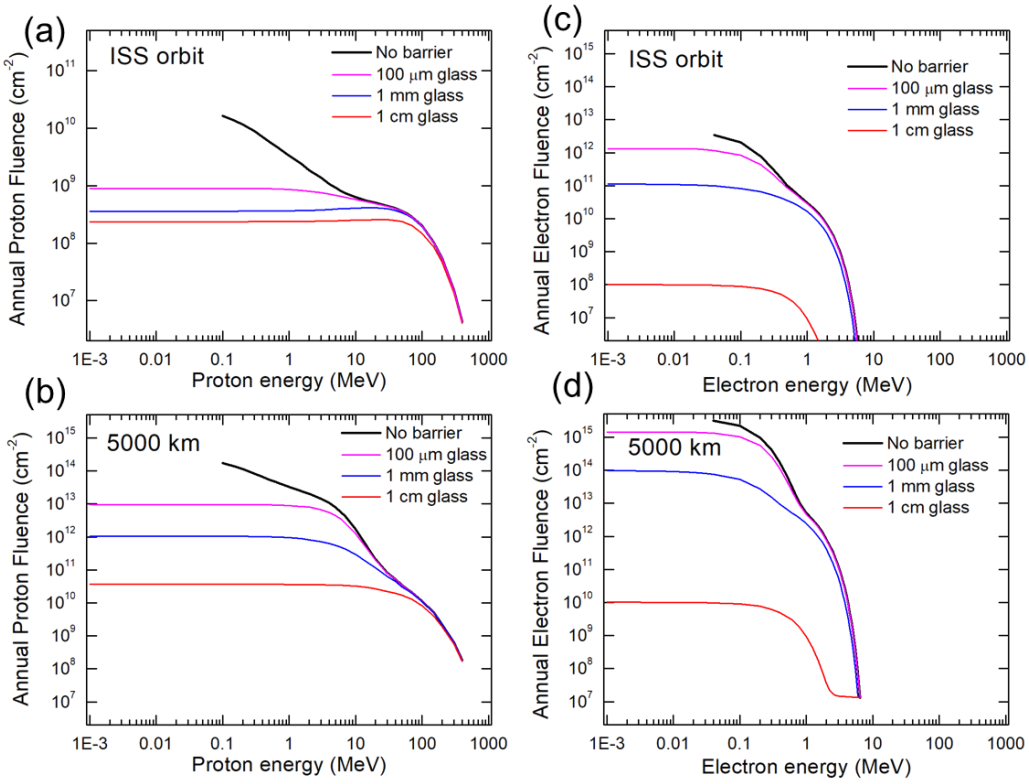

Figure S1. Slowed Proton Fluences for Various Cover Glass Thicknesses. Slowed spectra for proton fluences in (a) ISS orbit, and (b) a 5000 km altitude orbit (60° inclination), and electron fluences in (c) ISS orbit, and (d) a 5000 km altitude orbit (60° inclination). Various cover glass thicknesses are considered. The fluences without any barrier are shown in thick black lines. The original spectra were obtained using SPENVIS, while the slowed spectra with barriers were simulated using www.sr-niel.org

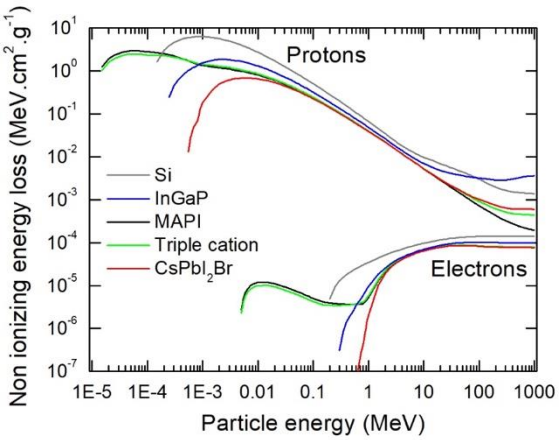

Figure S2. NIELs using SR-NIEL.org. NIELs simulated using www.sr-niel.org showing similarity with Figure 2a which uses SPENVIS.

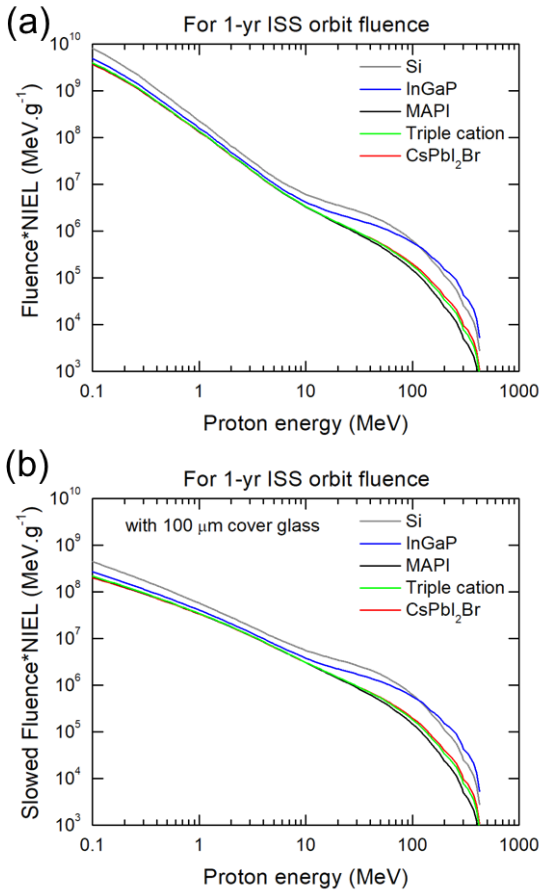

Figure S3. 1-yr ISS Orbit Displacement Damage Dose (DDD) Curves for Protons. DDD curves calculated by multiplying (a) unshielded proton fluences (Figure 1c), and (b) slowed fluences from protons shielded by 100 μm cover glass (Figure S1a), with NIELs (Figure 2c) for the ISS orbit.

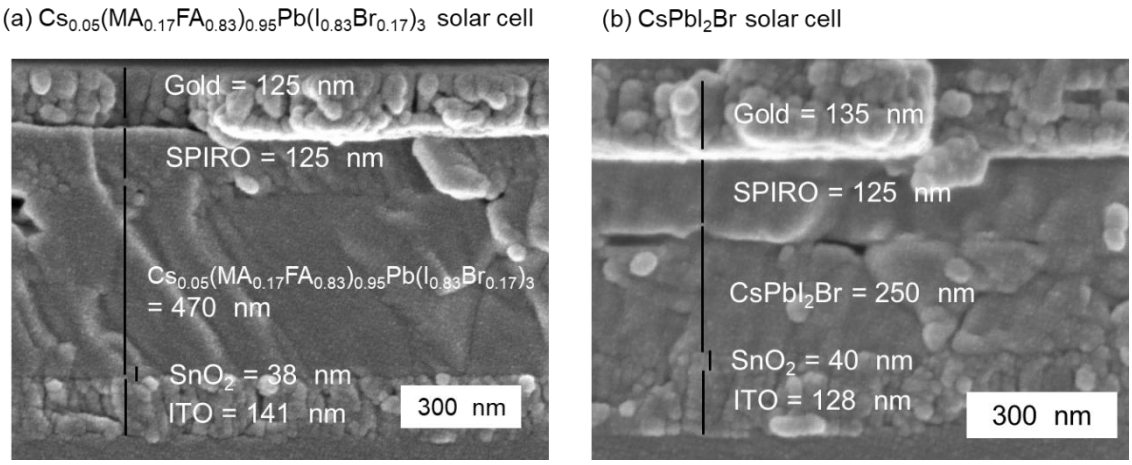

Figure S4. Cross-sectional SEM images. Cross-sectional SEM images of (a) $CsPbI_2Br$, and (b) $Cs_{0.05}(MA_{0.17}FA_{0.83})_{0.95}Pb(I_{0.83}Br_{0.17})_3$ solar cells showing thicknesses of various layers in the device stack. Film thicknesses used in SRIM/TRIM simulations in this paper are based on these experimentally-measured film thicknesses.

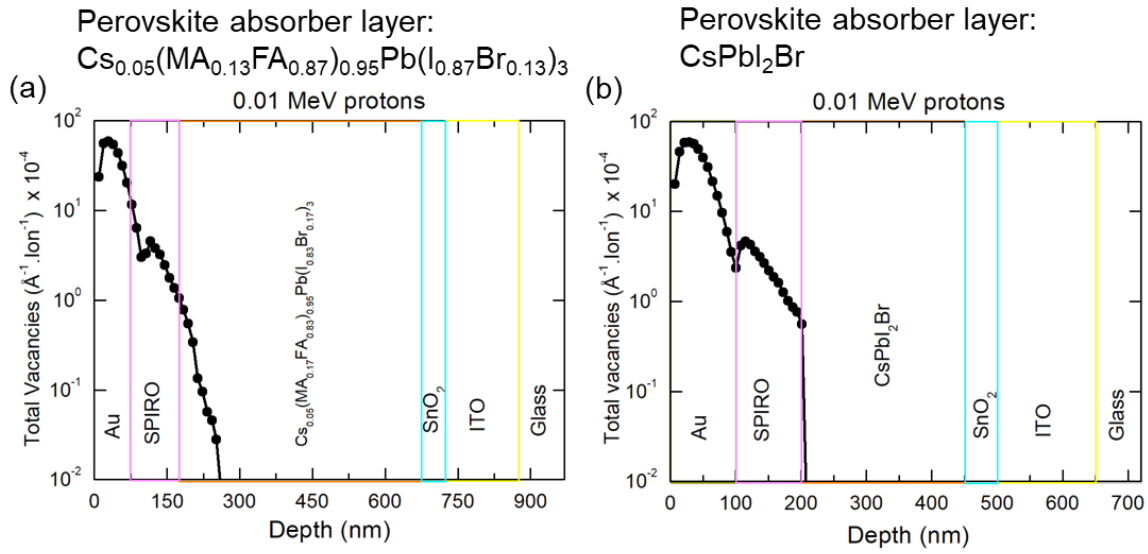

Figure S5. Vacancy Creation from 0.01 MeV Protons. Vacancies created by 0.01 MeV protons in (a) $CsPbI_2Br$ solar cell, (b) $Cs_{0.05}(MA_{0.17}FA_{0.83})_{0.95}Pb(I_{0.83}Br_{0.17})_3$ solar cell. Since these protons fail to reach the perovskite absorber due to their low energy, majority of the vacancies are confined to the metal electrode.

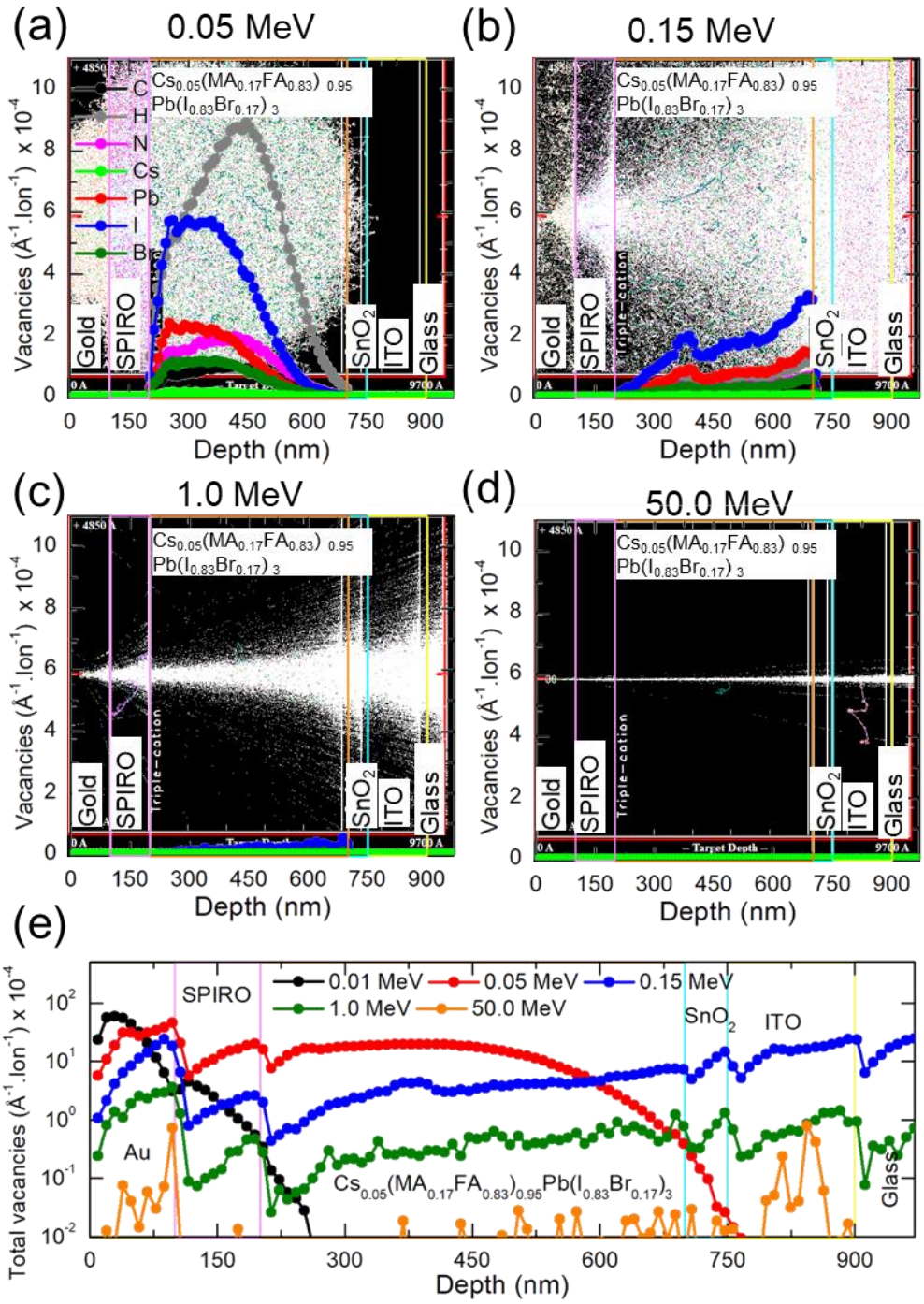

Figure S6. Simulated Proton Interaction with $Cs_{0.05}(MA_{0.17}FA_{0.83})_{0.95}Pb(I_{0.83}Br_{0.17})_3$ Perovskite Devices. a-d). Simulated proton straggling and the resulting vacancies formed due to dislocations of C, H, N, Cs, Pb, I, and Br atoms in $Cs_{0.05}(MA_{0.17}FA_{0.83})_{0.95}Pb(I_{0.83}Br_{0.17})_3$ solar cells. e). Vacancies formed in the full device stack. See Discussion below for details. Device architecture

considered is: Au (100 nm)/SPIRO (100 nm)/$Cs_{0.05}(MA_{0.17}FA_{0.83})_{0.95}Pb(I_{0.83}Br_{0.17})_3$ (500 nm)/SnO_2 (50 nm)/ITO (150 nm)/glass (70 nm).

Discussion:

The case of 0.05 MeV protons highlights the high frequency of collision events for these protons. In fact, these protons are found to stop within the solar cell causing significant displacements. 0.15 MeV protons show a reduced level of interactions, while 1 MeV proton transmit through the solar cells depositing minimal energy in the perovskite. 50 MeV protons are found to leave the solar cells almost unscathed. As expected, 0.05 MeV protons result in the most vacancies, while 50 MeV protons do not appear to create any significant concentration of vacancies in the absorber. Vacancies created in the full device stack are shown as a function of the device thickness/depth in Figure 4e. As can be seen, the 50 MeV protons create ~1000x less vacancies in the perovskite absorber compared to 0.05 MeV protons, in agreement with the NIEL calculated in Figure 2a.

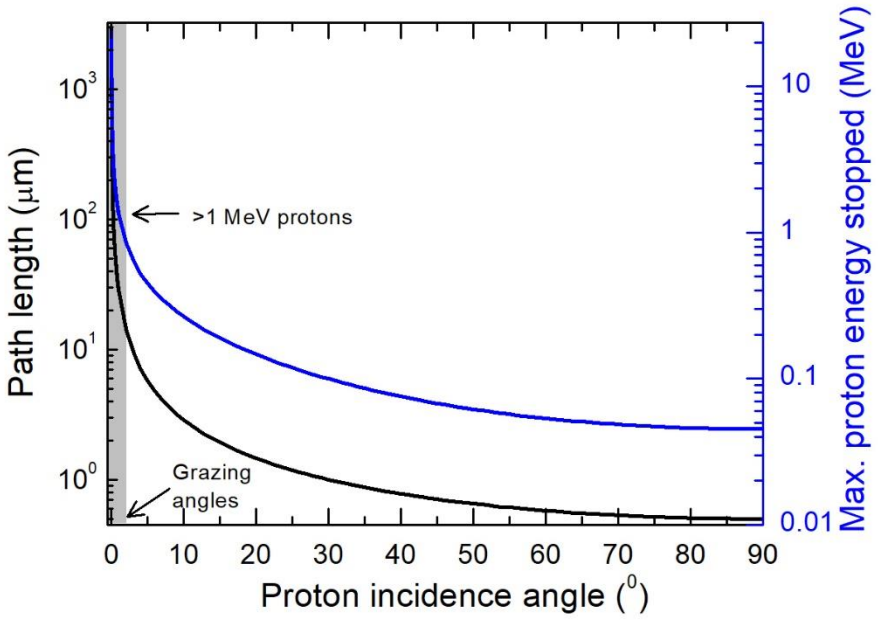

Figure S7. Proton Path Lengths *vs.* Incident Angle. Calculated proton path lengths as a function of incident angle. Right Y-axis shows the proton energies these path lengths (stopping range) correspond to. These are the maximum energies that will completely stop in the device stack at the calculated path lengths. As an example, normal incidence (90°) corresponds to a path length of 0.5 μm, which can stop a proton of ~0.045 MeV. Any higher energy proton will escape the solar cell. As the angles reduce and go toward the grazing-incidence scenario (0°), path lengths increase very slowly. 0.01° corresponds to a ~10,000 μm path length, which is the stopping range for 50 MeV

protons. However, such low incidence angles represent a very small fraction of all the angles possible. Most of the incidence scenarios are similar to the normal incidence case. In other words, for most of the incident angles, >0.05 MeV protons will escape the device and high-energy protons will create little damage.

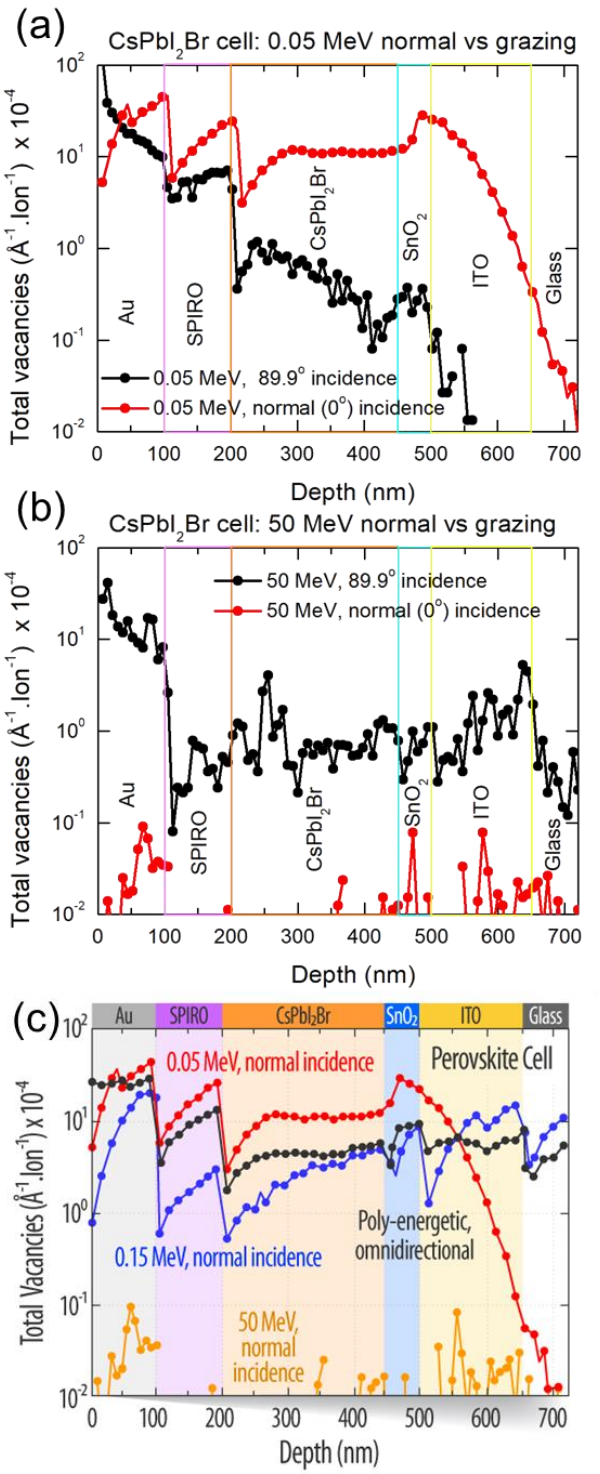

Figure S8. Vacancy Creation for Various Proton Incidence Angles. Damage profiles in a perovskite solar cell upon normal incidence (red) and grazing incidence (black) of (a) 0.05 MeV, and (b) 50 MeV protons, simulated using SRIM. (c) Irradiation of a $CsPbI_2Br$ solar cell with poly-energetic, omnidirectional protons. Normal incidences of 0.05, 0.15, and 50 MeV protons are also shown.

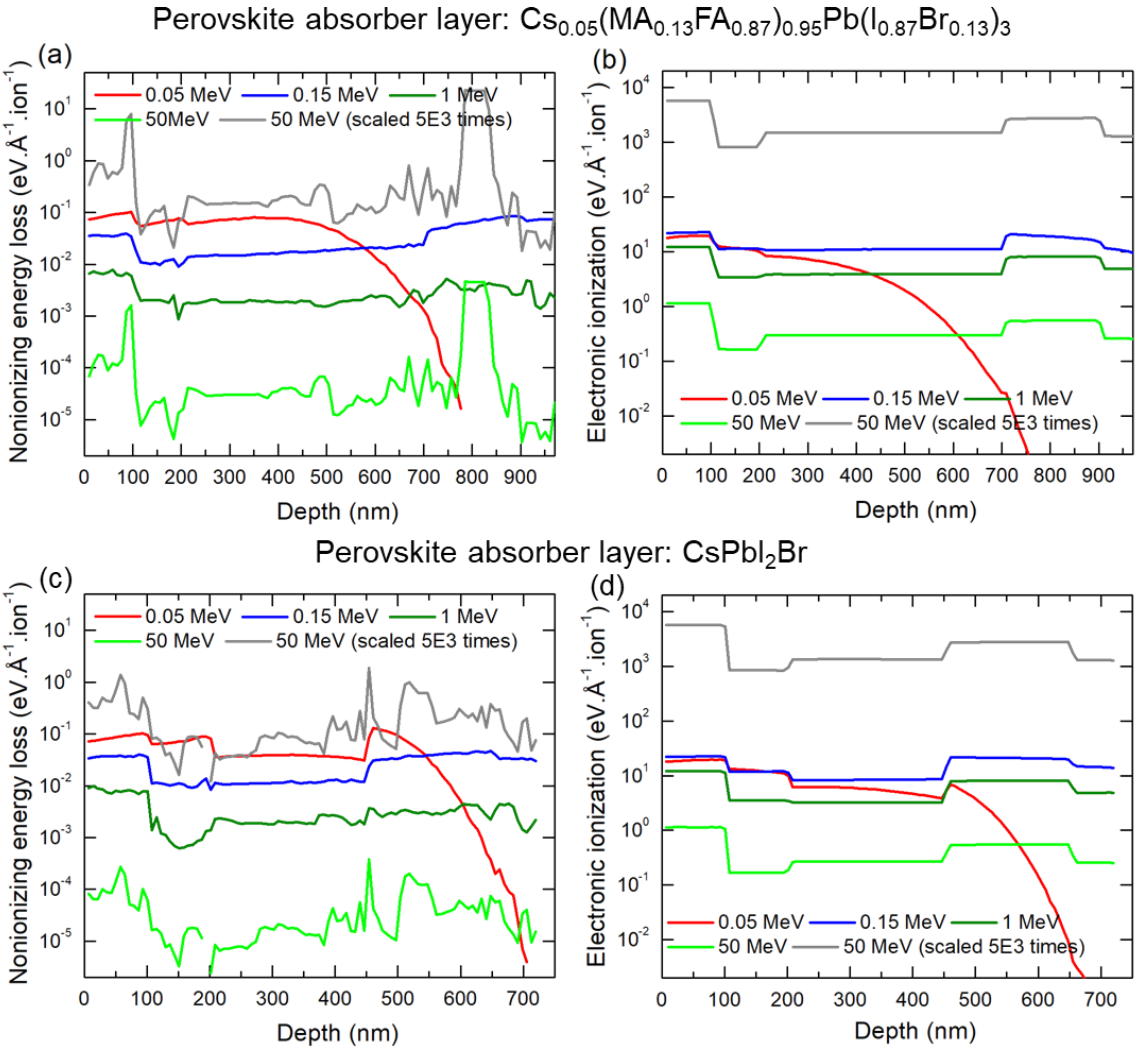

Figure S9. Simulated NIEL vs IEL in Perovskite Devices. SRIM/TRIM simulation results showing a) non-ionizing energy losses, and b) electronic ionization losses for 0.05, 0.15, 1 and 50 MeV protons in a $Cs_{0.05}(MA_{0.17}FA_{0.83})_{0.95}Pb(I_{0.83}Br_{0.17})_3$ solar cell with device architecture: Au (100 nm)/SPIRO (100 nm)/ $Cs_{0.05}(MA_{0.17}FA_{0.83})_{0.95}Pb(I_{0.83}Br_{0.17})_3$ (500 nm)/SnO_2 (50 nm)/ITO (150 nm)/glass (70 nm). Data for a $CsPbI_2Br$ solar cell with a device architecture: Au (100 nm)/SPIRO (100 nm)/ $CsPbI_2Br$ (250 nm)/SnO_2 (50 nm)/ITO (150 nm)/glass (70 nm) are shown in (c) and (d). Both loss mechanisms scale differently with fluence (number of ions). 5E3 protons of 50 MeV (grey spectra) will create a similar number of nuclear displacements as 1 proton of 0.05

MeV (panel a, c), however the corresponding electronic ionization (healing) will be much higher (panel b, d). This implies that fluence at one energy cannot be scaled to match the fluence at another energy in terms of damage induced.

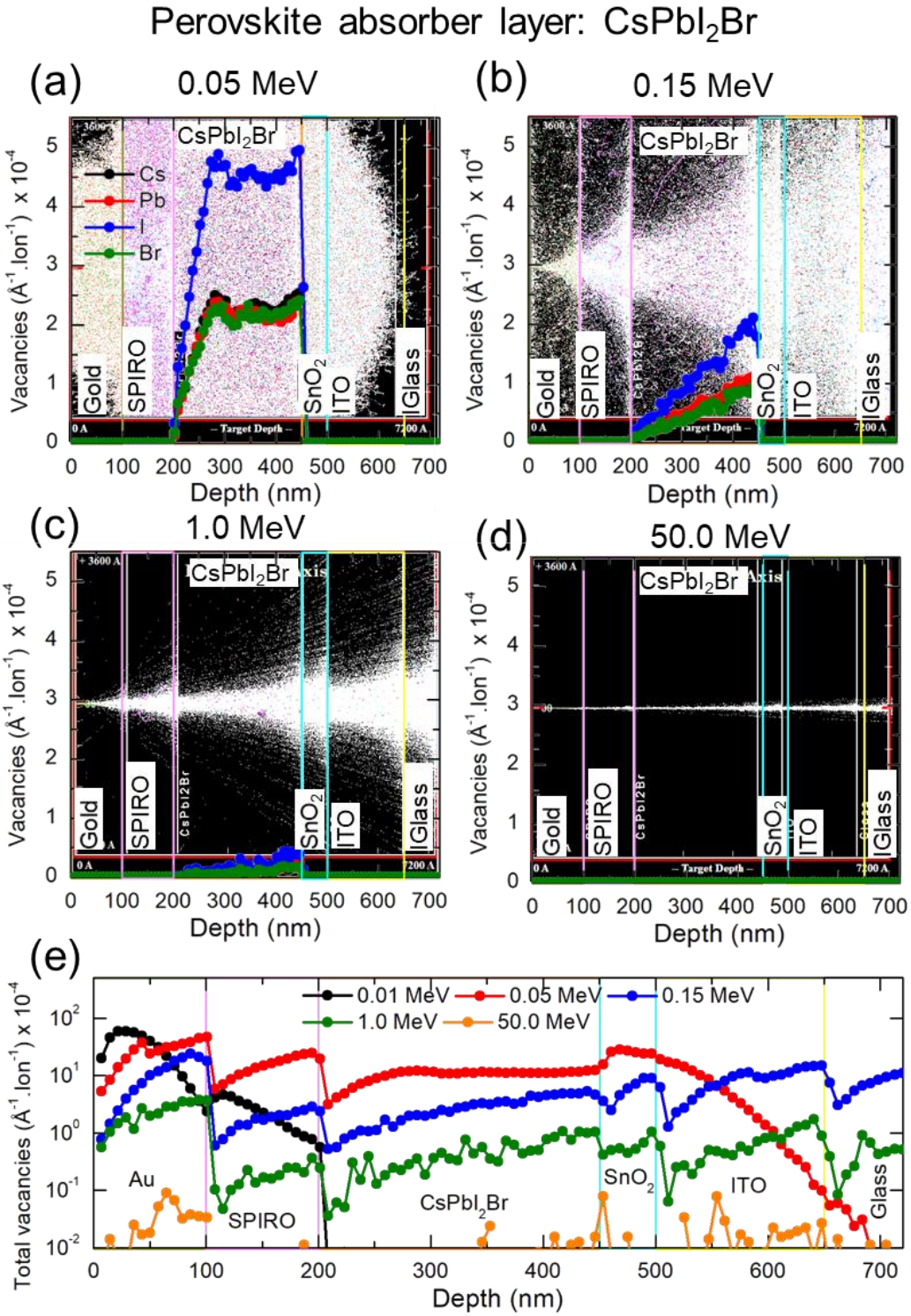

Figure S10. Simulated Proton Interaction with $CsPbI_2Br$ Perovskite Devices. a-d). Simulated proton straggling and the resulting vacancies formed due to dislocations of I, Br, Cl and Br atoms in $CsPbI_2Br$ solar cells. e). Vacancies formed in the full device stack. See Discussion below for details. Device architecture considered is: Au (100 nm)/SPIRO (100 nm)/$CsPbI_2Br$ (250 nm)/SnO_2 (50 nm)/ITO (150 nm)/glass (70 nm).

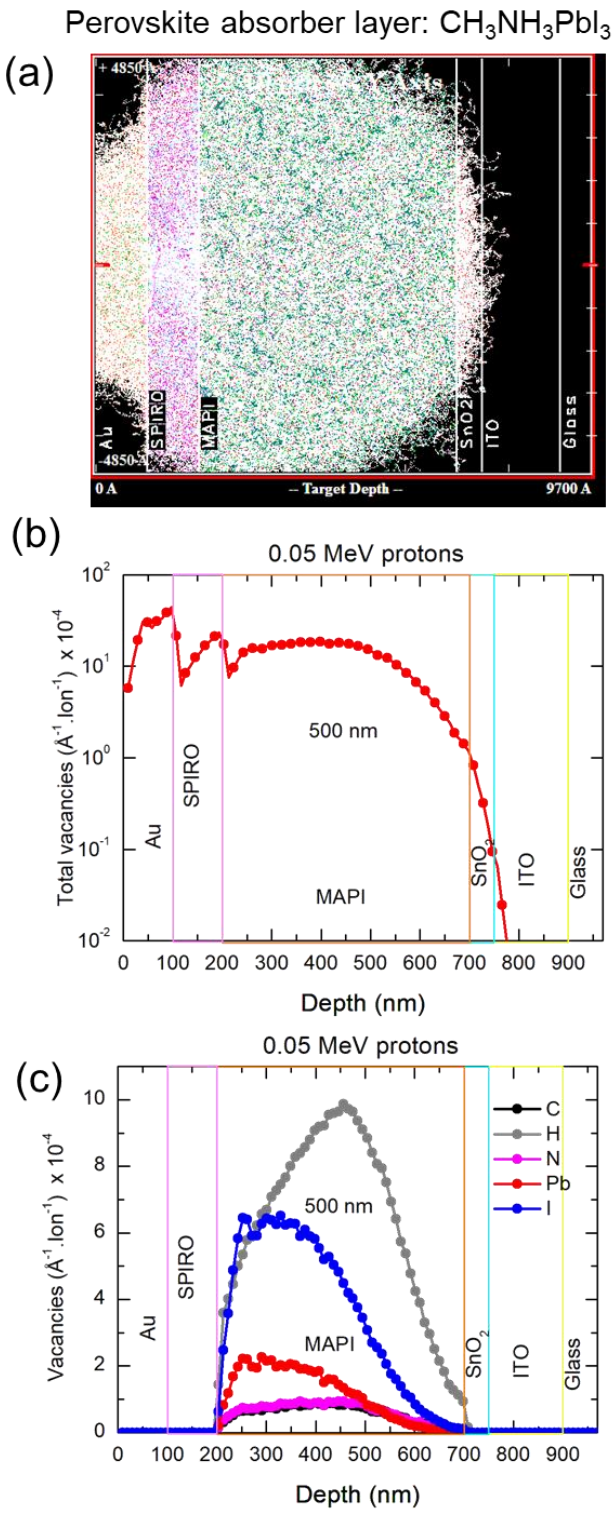

Figure S11. Simulated Proton Interaction with a $CH_3NH_3PbI_3$ Perovskite Device. (a) Proton straggling for $CH_3NH_3PbI_3$ solar cells, (b) vacancies created in the device, and (c) vacancies due to C, H, N, Pb, and I. Device structure considered is: Au (100 nm)/SPIRO (100 nm)/$CH_3NH_3PbI_3$ (500 nm)/SnO_2 (50 nm)/ITO (150 nm)/glass (70 nm).

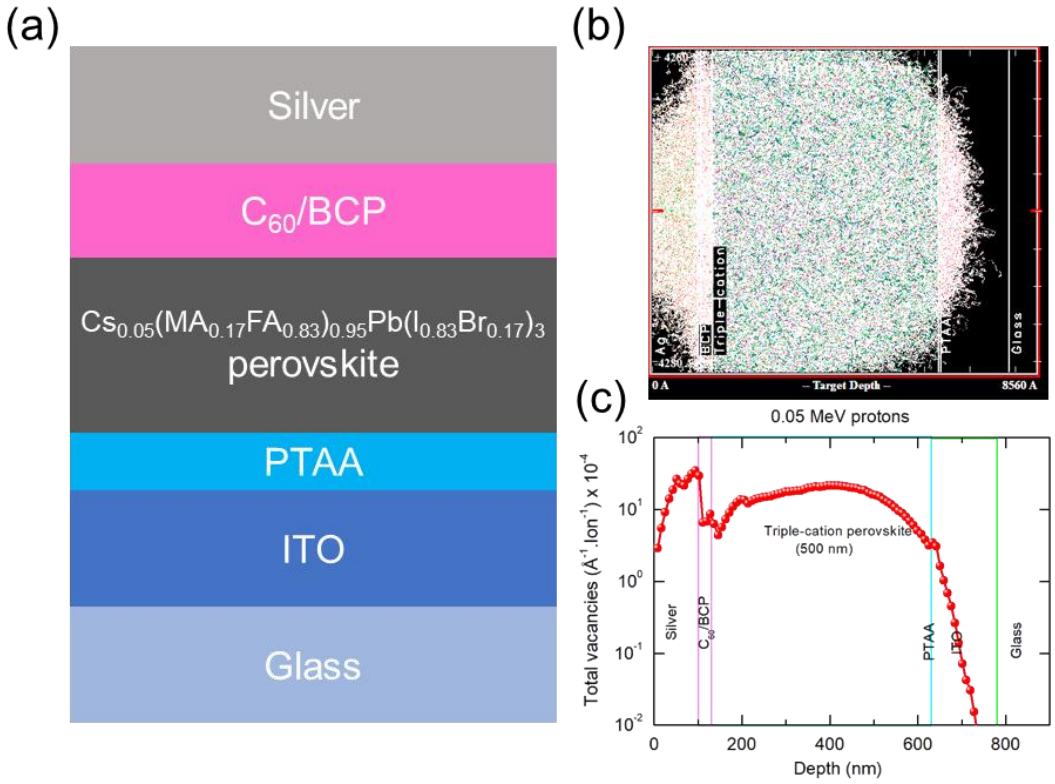

Figure S12. Simulated Proton Interaction with a *PIN* Perovskite Device. Proton interactions in a *pin* $Cs_{0.05}(MA_{0.17}FA_{0.83})_{0.95}Pb(I_{0.83}Br_{0.17})_3$ solar cell. (a) Device architecture considered for modeling. (b) SRIM/TRIM simulations showing straggling of 0.05 MeV protons incident from the silver electrode side. (c) Red line represents the total vacancies generated within the device stack and highlights that 0.05 MeV protons create a majority of vacancies inside the perovskite active layer, similar to the case of $CsPbI_2Br$ and *n-i-p* $Cs_{0.05}(MA_{0.17}FA_{0.83})_{0.95}Pb(I_{0.83}Br_{0.17})_3$ solar cells solar cells.

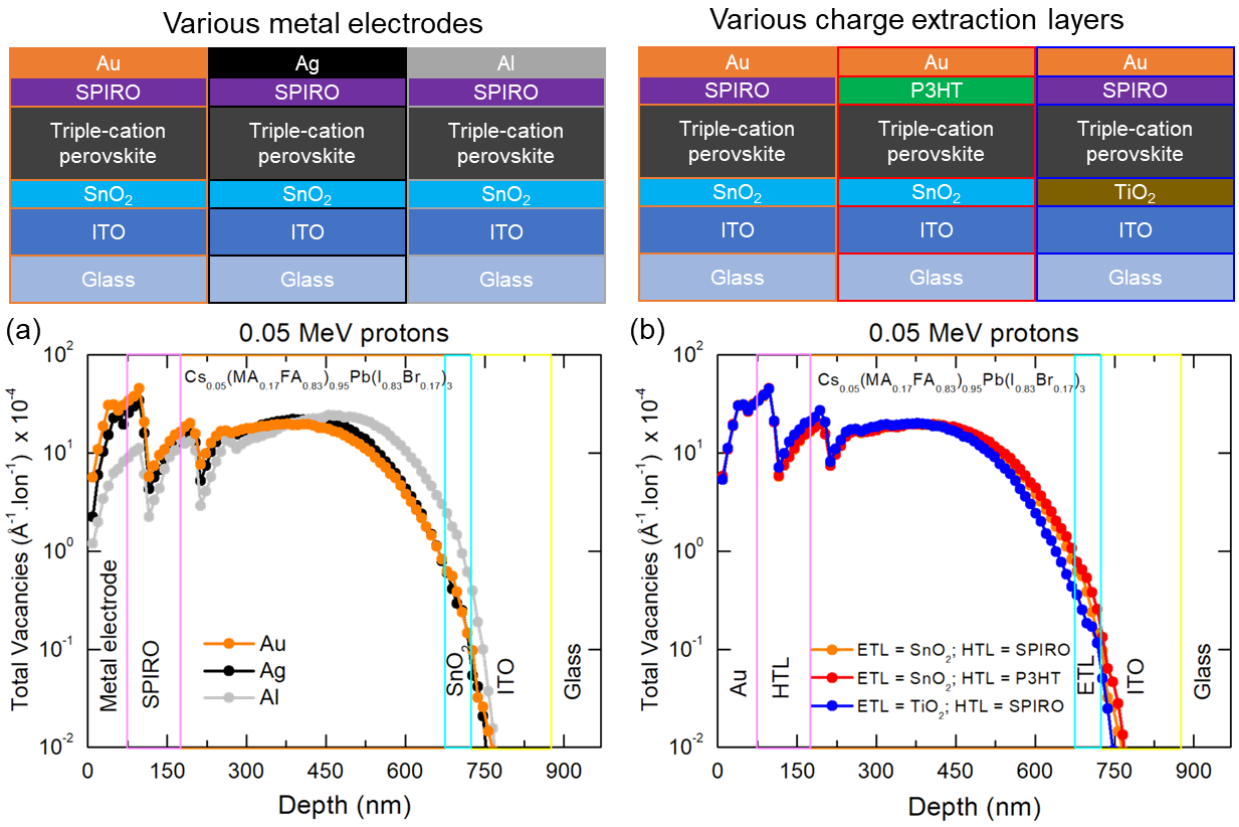

Figure S13. Vacancy Creation in Various Perovskite Device Architectures. SRIM simulations showing vacancy profiles within device stacks with (a) different metal electrodes, and (b) different charge extraction layers. Device stacks considered are shown in schematics above the figures.

Discussion:

Given the importance of metal electrode and charge extraction layers in the device stack, we also performed SRIM simulations on $Cs_{0.05}(MA_{0.17}FA_{0.83})_{0.95}Pb(I_{0.83}Br_{0.17})_3$ perovskite device stacks with various metal contacts (Ag and Al), a different hole-transporting layer (P3HT), and a different electron-transporting layer (TiO_2) to understand interaction of protons with these layers and defect formation. The vacancy profiles in these device stacks upon irradiation with 0.05 MeV protons are shown in Figure S13. Protons are found to create the smallest number of vacancies in the Al electrode compared to Au and Ag. Although Al has a significanty smaller atomic number ($Z = 13$) and its atoms have low binding strength compared to Au ($Z = 79$) and Ag ($Z = 47$), it has a vastly lower mass density of 2.7 g.cm^{-3} than Au (19.3 g.cm^{-3}) and Ag (10.49 g.cm^{-3}). A low mass density results in a smaller number of Al atoms per unit volume reducing the probability of interaction with protons. This implies that the incident protons do not lose sufficient energy while passing

through Al and can create more damage upon reaching the perovskite absorber. In fact, Figure S13a shows that for the perovskite solar cell with Al electrode has a larger number of vacancies inside the perovskite layer. This can potentially mean that Ag and Au electrodes can limit proton damage to the perovskite.

Similarly, given its higher mass density (1.4 $g.cm^{-3}$), SPIRO has higher vacancy profile compared to the lower mass density P3HT (1.1 $g.cm^{-3}$). As expected, perovskite active layer in the SPIRO device shows slightly less vacancies than the case of P3HT (Figure S13b). It is harder to compare electron transporters given that protons pass through them after traversing the perovskite, meaning their interaction with electron transporter layers does not affect the vacancy profile within the perovskite.

Table S1. Proton look-up table for ISS orbit.

Proton Energy (MeV)	**1-yr Fluence (cm^{-2})**	**5-yr Fluence (cm^{-2})**	**20-yr Fluence (cm^{-2})**	**1-yr DDD ($MeV.g^{-1}$)**				
				Triple-cation	MAPI	$CsPbI_2Br$	Si	InGaP
0.10	1.6E10	8.1E10	3.2E11	4.0E9	3.9E9	3.7E9	8.2E9	4.9E9
0.150	1.4E10	6.8E10	2.7E11	2.5E9	2.4E9	2.3E9	4.9E9	3.0E9
0.500	5.9E9	3.0E10	1.2E11	4.2E8	4.2E8	4.1E8	7.5E8	5.0E8
1.000	3.3E9	1.7E10	6.7E10	1.3E8	1.3E8	1.3E8	2.2E8	1.6E8
50.000	3.6E8	1.8E9	7.3E9	5.4E5	4.8E5	5.5E5	1.7E6	1.2E6
100.000	2.0E8	1.0E9	4.0E9	1.8E5	1.5E5	2.0E5	6.2E5	5.7E5

Discussion: Equivalent fluences can be calculated from the DDD values at two different proton energies. As an illustration, a fluence of 1.6E10 cm^{-2} for 0.10 MeV protons will result in a similar nuclear displacement damage in a $Cs_{0.05}(MA_{0.17}FA_{0.83})_{0.95}Pb(I_{0.83}Br_{0.17})_3$ solar cell as (4.0E9/1.8E5)*1.6E10 = 3.6E14 cm^{-2} fluence for 100 MeV protons. However, this 100 MeV proton fluence should not be used to simulate the effect of 0.10 MeV protons, since the electronic ionization (healing) scales differently. 100 MeV protons at a fluence of 3.6E14 cm^{-2} create significantly higher electronic ionization events than 1.6E10 cm^{-2} fluence of 0.10 MeV protons.

Indeed, the reverse is also true and lower energy protons should not be used for high-energy equivalence.

Annual fluences for various proton energies in equivalents of 0.1 MeV protons are calculated and shown in Table S2 for various PV technologies.

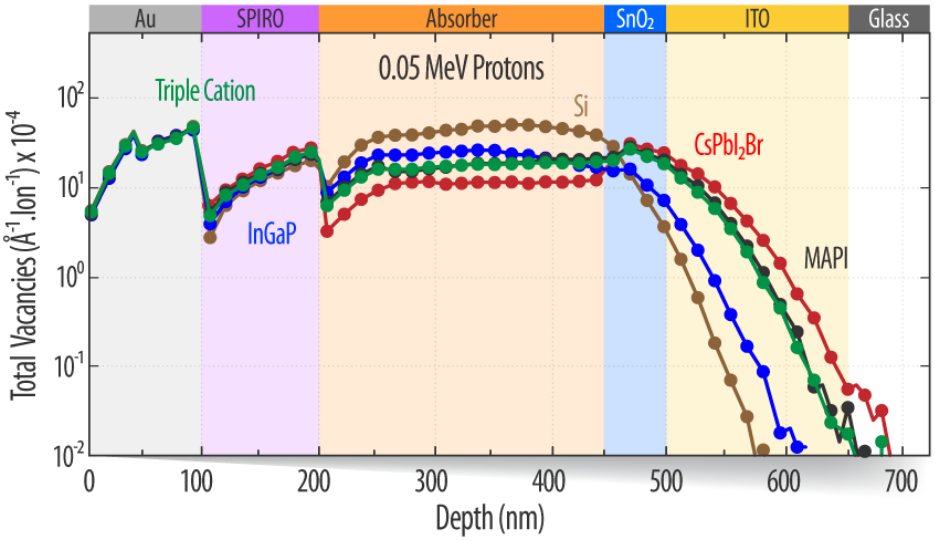

Figure S14. Defect Creation in Various Solar Cell Technologies. Comparison of vacancies formed in device stacks with perovskite absorbers ($Cs_{0.05}(MA_{0.17}FA_{0.83})_{0.95}Pb(I_{0.83}Br_{0.17})_3$, $CH_3NH_3PbI_3$, and $CsPbI_2Br$) and conventional PV absorbers (Si and InGaP), upon irradiation with 0.05 MeV protons and assuming constant thickness absorber.

Table S2. Equivalent annual fluences for ISS orbit for various PV technologies.

Proton Energy (MeV)	**1-yr Fluence (cm^{-2})**	**0.1 MeV Equivalent Annual Fluence (cm^{-2})**				
		Triple-cation	MAPI	$CsPbI_2Br$	Si	InGaP
0.10	1.6E10	1.6E+10	1.6E+10	1.6E+10	1.6E+10	1.6E+10
0.150	1.4E10	2.6E+10	2.6E+10	2.6E+10	2.7E+10	2.6E+10
0.500	5.9E9	1.5E+11	1.5E+11	1.4E+11	1.8E+11	1.6E+11
1.000	3.3E9	4.9E+11	4.8E+11	4.6E+11	6.0E+11	4.9E+11
50.000	3.6E8	1.2E+14	1.3E+14	1.1E+14	7.7E+13	6.5E+13
100.000	2.0E8	3.6E+14	4.2E+14	3.0E+14	2.1E+14	1.4E+14

Table S3. **Proton Energies Adjusted for Various Cover Glass Thicknesses.** Proton energies suggested for irradiation of perovskite solar cells after including a cover glass in the device stack. Proton energies in bold correspond to the reduced energies incident on the top metal electrode after the protons pass through the cover glass.

Cover glass thickness (μm)	**Proton energy (MeV) after 'cover glass correction'**				
	0.050	**0.075**	**0.100**	**0.150**	**0.200**
50	2.368	2.393	2.418	2.468	2.518
100	3.491	3.516	3.541	3.591	3.641
150	4.562	4.587	4.612	4.662	4.712
200	5.455	5.480	5.505	5.555	5.605
1000	13.457	13.482	13.507	13.557	13.607